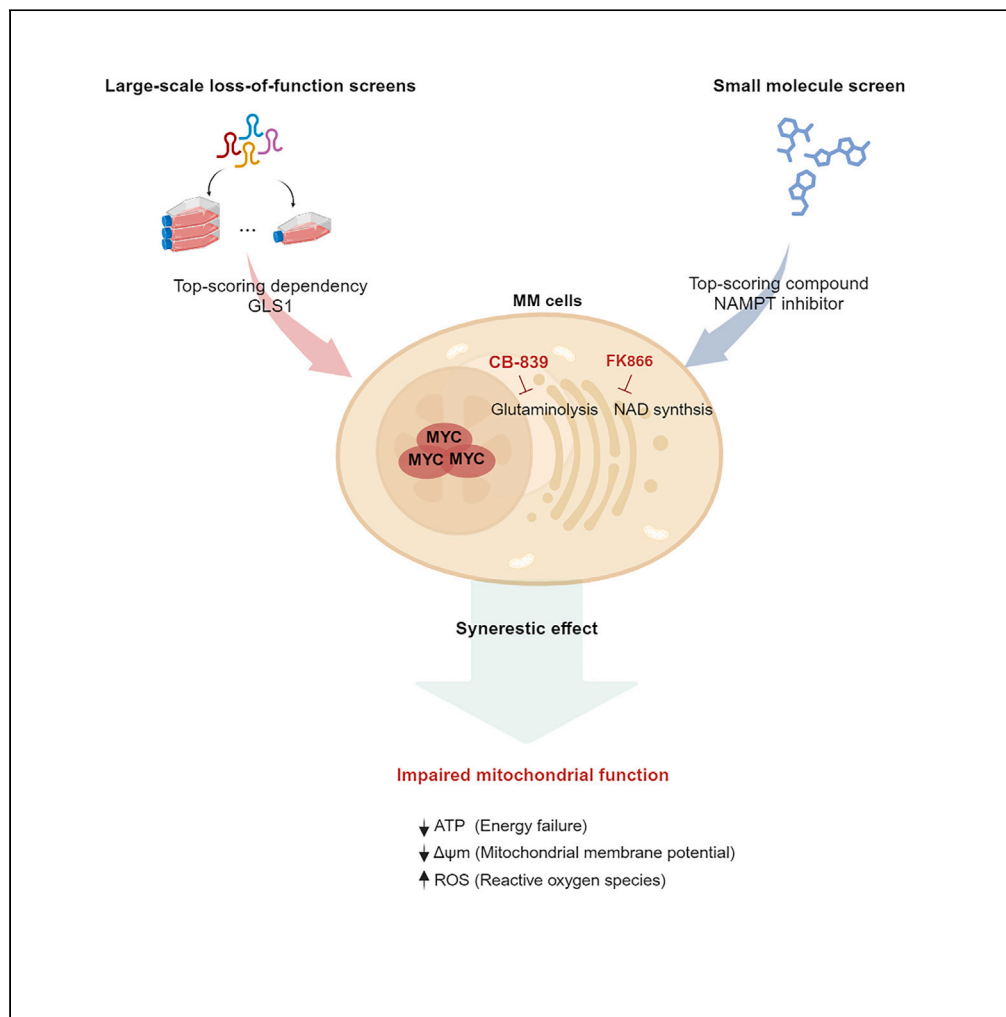


Article

MYC dependency in GLS1 and NAMPT is a therapeutic vulnerability in multiple myeloma



Lama Hasan Bou Issa, Léa Fléchon, William Laine, ..., Irene M. Ghobrial, Jérôme Kluza, Salomon Manier

salomon.maniem@inserm.fr

Highlights

MYC overexpressing (MYC OE) cells are selectively dependent on glutaminase (GLS1)

GLS1 dependency in MYC-driven cells is non-oncogenic

CB-839 reduces OXPHOS and cellular biosynthesis and has anti-tumor effect in MM

GLS1 inhibition synergizes with NAMPT inhibition to block OXPHOS in MYC OE MM

Hasan Bou Issa et al., iScience
27, 109417
April 19, 2024 © 2024 The Author(s).
<https://doi.org/10.1016/j.isci.2024.109417>

Article

MYC dependency in GLS1 and NAMPT is a therapeutic vulnerability in multiple myeloma

Lama Hasan Bou Issa,¹ Léa Fléchon,¹ William Laine,¹ Aicha Ouelkdite,¹ Silvia Gaggero,¹ Adeline Cozzani,¹ Remi Tilmont,² Paul Chauvet,² Nicolas Gower,² Romanos Sklavenitis-Pistofidis,³ Carine Brinster,¹ Xavier Thuru,¹ Yasmine Touil,¹ Bruno Quesnel,^{1,2} Suman Mitra,¹ Irene M. Ghobrial,³ Jérôme Kluza,¹ and Salomon Manier^{1,2,4,*}

SUMMARY

Multiple myeloma (MM) is an incurable hematological malignancy in which MYC alterations contribute to the malignant phenotype. Nevertheless, MYC lacks therapeutic druggability. Here, we leveraged large-scale loss-of-function screens and conducted a small molecule screen to identify genes and pathways with enhanced essentiality correlated with MYC expression. We reported a specific gene dependency in glutaminase (GLS1), essential for the viability and proliferation of MYC overexpressing cells. Conversely, the analysis of isogenic models, as well as cell lines dataset (CCLE) and patient datasets, revealed GLS1 as a non-oncogenic dependency in MYC-driven cells. We functionally delineated the differential modulation of glutamine to maintain mitochondrial function and cellular biosynthesis in MYC overexpressing cells. Furthermore, we observed that pharmaceutical inhibition of NAMPT selectively affects MYC upregulated cells. We demonstrate the effectiveness of combining GLS1 and NAMPT inhibitors, suggesting that targeting glutaminolysis and NAD synthesis may be a promising strategy to target MYC-driven MM.

INTRODUCTION

Multiple myeloma (MM) is a plasma cell malignancy characterized by the proliferation of monoclonal plasma cells in the bone marrow. MM accounts for approximately 13% of all hematological cancers.¹ The disease passes through precursor or asymptomatic stages, with monoclonal gammopathy of undetermined significance (MGUS) and smoldering multiple myeloma (SMM).^{2,3} While MM oncogenesis is initiated by primary genetic events, mainly hyperdiploidy and immunoglobulin heavy chains (IgH) translocations, secondary genetic events play a major part in the disease progression.⁴⁻⁶ MYC translocations are among the most recurrent secondary aberrations in newly diagnosed MM patients. Mainly translocation t(8; 14), in which the MYC (8q24) juxtaposes the IgH enhancer on the derivative chromosome 14 leading to MYC overexpression.^{5,7-9} MYC protein dimerizes with its obligatory partner MAX to bind to the E-box element (CACGTG) and function as a sequence-specific DNA-binding transcription factor.¹⁰ MYC is a master regulator of numerous key biological activities, including cell growth, cell cycle, and metabolism. MYC expression being a common property of all proliferating cells, the intrinsically disordered location of its main functional domains in addition to the protein localization inside the nucleus and its short half-life, collectively these properties raise the challenge to find innovative ways to target MYC without causing unacceptable toxicities.^{11,12}

Certain pathways in cancer cells have increased importance compared to normal cells in the interest of buffering different stress levels, such as replication stress, or DNA damage. These pathway dependencies also provide exploitable vulnerabilities to cancer cells, which can be targeted for therapeutic interventions. This approach can result in stress overload and apoptosis of cancer cells while sparing normal cells. In this regard, cancer dependencies are receiving greater interest to uncover genes with enhanced essentiality in a specific cellular context. Here, we hypothesized that the proliferative advantage promoted by MYC overexpression induces differential genomic dependencies on particular signaling pathways, thus creating vulnerabilities with potential therapeutic relevance.

To test this hypothesis, we applied large-scale, unbiased approaches to identify vulnerabilities in MYC overexpressing MM cells by exploiting cancer dependency map and conducting small molecule screening. We report specific dependencies of MYC overexpressing cells on glutaminase (GLS1) and nicotinamide phosphoribosyltransferase (NAMPT) in MM. GLS1 is pivotal in glutamine metabolism, which catalyzes the conversion of glutamine into glutamate and ammonia.^{13,14} NAMPT is a key enzyme in the NAD salvage pathway, which recycles

¹Canther, INSERM UMR-S1277 and CNRS UMR9020, Lille University, 59000 Lille, France

²Department of Hematology, CHU Lille, 59000 Lille, France

³Dana-Farber Cancer Institute, Harvard Medical School, Boston, MA 02215, USA

⁴Lead contact

*Correspondence: salomon.manier@inserm.fr

<https://doi.org/10.1016/j.isci.2024.109417>



nicotinamide (NAM) back into NAD.¹⁵ The fate of glutamine and NAD are tightly interconnected, involved in various aspects of cellular bioenergetics and adaptation to hypoxic conditions. We further observed a synergistic activity of the dual inhibition of GLS1 and NAMPT in MM. Together, our data demonstrated that combinatorial treatment of CB-839 and FK-866 constitutes a potential novel therapeutic strategy against MM in the context of MYC upregulation.

RESULTS

MYC overexpression in MM growth is dependent on GLS1 activity

We searched for genomic vulnerabilities associated with MYC overexpression by leveraging genome-scale pooled shRNA screening data in a panel of 236 cancer cell lines from Project Achilles to identify the genes essential for proliferation and survival of high MYC-expressing cell lines. MYC expression level for each cell line was determined using expression profile data from the Cancer Cell Line Encyclopedia (CCLE). We correlated 54,393 shRNA sensitivity profiles with MYC expression level identified four shRNAs that strongly correlated with reduced viability in MYC-high but not MYC-low cells: MAX ($r = -0.51$, $p < 0.001$), an obligate partner of MYC representing an internal validation of our method, followed by GLS1 ($r = -0.48$, $p < 0.001$) and SLC1A1 ($r = -0.42$, $p < 0.001$), encode the rate-limiting enzyme in glutamine metabolism (glutaminase) and cytoplasmic glutamine transporter, respectively (Figure 1A; Table S1). This correlation between the sensitivity to shGLS1, shSLC1A1 and MYC expression level demonstrated a selective dependency on glutamine metabolism in the context of MYC overexpression. Since MYC is a powerful driver gene that modulates the expression of numerous genes, we defined MYC gene signature score (Z score) derived from the expression of hallmark MYC target v2 (58 genes).¹⁶ We correlated Z score to the shRNA sensitivity profiles from Project Achilles to identify differential genomic dependencies that correlate with MYC signature. Our analysis revealed that the higher score of MYC target v2 is associated with higher GLS1 dependency (Figure 1B; Table S2). Due to the rarity of MM cell lines with low MYC expression level, we generated an MM isogenic model overexpressing MYC in U266 cell line transduced with EF1A-C-MYC lentiviral vector (Figures S1A and S1B). For validation, we introduced two distinct doxycycline-inducible shGLS1 in order to induce depletion of GLS1. Both shGLS1#1 and shGLS1#2 caused a selective reduction in proliferation of U266/MYC cells over U266/Ctrl cells (Figures 1C and S1C). We also observed a higher sensitivity to glutamine-deprived conditions of MYC-high cells as compared to MYC-low cells (Figure S1D). We used pharmacological inhibition of the glutamine metabolism pathway for further validation. CB-839, a potent non-competitive inhibitor of GLS1, on a wide spectrum of cancer cell lines including MM, breast, colon, and lung cancer. Notably, we observed a strong negative correlation between CB-839 response and MYC expression level (Figures 1D and S1E). We also tested V-9302, a competitive antagonist of transmembrane glutamine transporter SLC1A5. Similarly, we observed a higher sensitivity of MYC-high cell to SLC1A5 inhibition (Figures 1E and S1F). Taken together, these results indicate that MYC overexpression confers higher dependency on glutamine metabolism pathway and confers enhanced sensitivity to pharmacological inhibition of GLS1.

GLS1 function as a non-oncogenic dependency

To further examine the relationship between MYC oncogenic signaling and glutamine dependency, we analyzed the transcriptome and translational profiles of the U266 isogenic model via RNA-seq and TMT mass tag, respectively. At the transcriptomic level, we identified 119 and 829 genes significantly up- or down-regulated with a fold change higher than 2 and a p value < 0.05 . Among the top-upregulated genes were genes related to cell cycle, including (*CDK6*; FC = 3.7, $p < 0.001$), (*ERCC6L*; FC = 2.17, $p < 0.001$), (*GEM*; FC = 2.87, $p < 0.001$), (*MYB*; FC = 2.68, $p < 0.001$), and glycolysis (*HK2*; FC = 5.4, $p < 0.001$), whereas several zinc finger transcription factors were among the most significantly down-regulated genes (Figure 2A; Table S3). On the protein level, our proteomics analysis identified 29 and 15 proteins significantly up- or down-regulated with a fold change higher or lower than 2, respectively, and a p value < 0.05 showed significant downregulation in the interferon type I signaling pathway (Figure 2B; Table S4). We next sought to test whether the enhanced dependency on GLS1 is due to an upregulation of glutamine metabolism-related genes. Interestingly, those genes were not significantly upregulated on either RNA or protein level (Figures 2C and 2D). Likewise, expression data from CCLE database derived from data for 169 hem cell lines indicated no significant upregulation of the glutamine metabolism-related genes (Figure 2E). To obtain further insights into the core enriched pathways in MYC overexpressing cells, we compared their enrichment in our isogenic model, in 169 hematological cell lines from CCLE, and in two independent patient datasets (GSE4452 - MMRF-CoMMpass). All datasets were grouped by MYC expression level. Gene set enrichment analysis (GSEA) consistently showed a correlation pattern with significant enrichment of ribosomal biogenesis and translational activity pathway, while no significant enrichment in the glutamine metabolism-related gene sets (Figures 2F–2I; Table S5). This is in line with the higher translational activity induced by MYC.^{17–20} Collectively, we show that MYC does not transcriptionally nor translationally upregulate glutamine metabolism pathway. These findings likely reflect a non-oncogenic dependency in MYC overexpressing cells on GLS1.

GLS1 inhibition selectively compromises the metabolic fitness of MYC OE cells

Initially, glutamine metabolism in the mitochondria and its conversion to CO₂ and H₂O is an oxygen-consuming process. This process is a major metabolic fate of glutamine and a primary source of bioenergy. Using the Seahorse XF analyzer we measured the kinetic oxygen consumption rate (OCR) response in U266/Ctrl and U266/MYC under glutamine supplement. U266/MYC cells possess the ability to oxidize glutamine at a higher rate compared to U266/Ctrl. Injecting CB-839 at 5 μM was able to abolish the glutamine-induced OCR in U266/MYC demonstrating the incapability of MYC OE cells to maintain sufficiently high level of oxidative phosphorylation (OXPHOS) under glutamine metabolism disruption (Figure 3A). Additionally, we assessed the effect of CB-839 and GLS1 knockdown on the mitochondrial function of

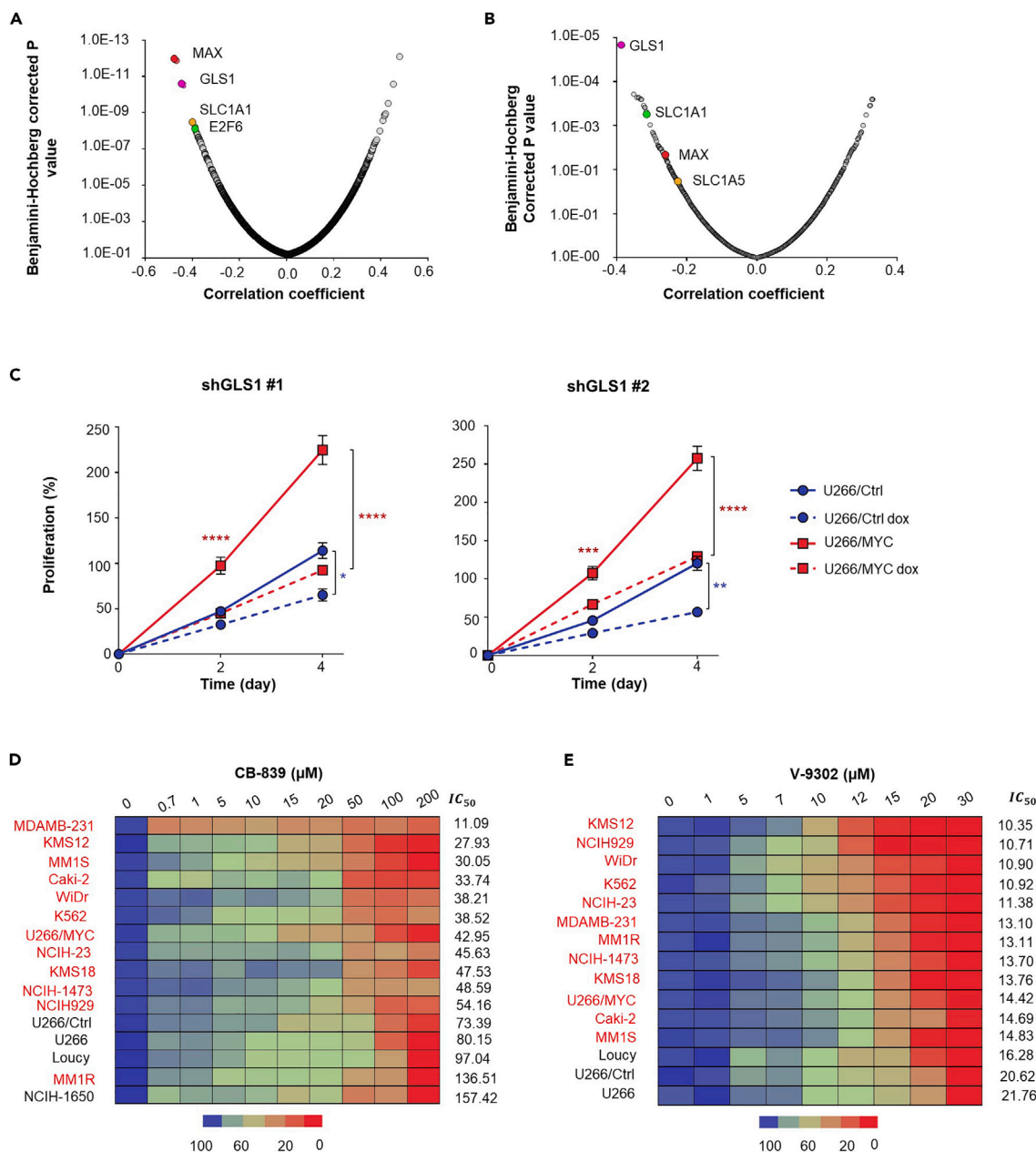


Figure 1. Interrogation of genome-scale pooled short hairpin RNA (shRNA) screening data to identify potential vulnerability in MYC overexpressing cells

(A) Point biserial correlation coefficients for association with MYC overexpression are blotted against Benjamini-Hochberg corrected p value for 54,393 shRNA. Genes scored as differentially lethal in MYC overexpressing cell lines were highlighted, MAX ($r = -0.51$, $p < 0.001$), GLS1 ($r = -0.48$, $p < 0.001$), SLC1A1 ($r = -0.42$, $p < 0.001$) and E2F6 ($r = -0.41$, $p < 0.001$).

(B) Point biserial correlation coefficients for association with MYC signature are blotted against Benjamini-Hochberg corrected p value for 54,393 shRNA.

(C) Analysis of proliferation of U266/Ctrl and U266/MYC transduced with a lentiviral vector expressing either an inducible (shGLS1#1) and (shGLS1#2) cultured with or without doxycycline for the indicated time in order to induce depletion of GLS1. * Indicates p values < 0.05 , ** indicates p value < 0.01 , *** indicates p value < 0.001 and **** indicates p value < 0.0001 ; one-way ANOVA with Tukey's test.

(D and E) Heatmap represents the dose-response effect in 13 human cancer cell lines of various cancers including: Breast cancer, MM, renal cancer, colon cancer, and lung cancer. Cell lines were treated with CB-839 (0–200 μM for 48 h) and V-9302 (0–30 μM for 48 h). The percentage survival (expressed as percentage of the DMSO-treated control) is visualized in color format according to their values on a linear scale (0–100%) and row-ranked by IC₅₀ values from lowest to highest. Cell lines with high MYC expression values were highlighted in red. Data in (C–E) are represented as mean \pm SEM of triplicates of three representative experiments.

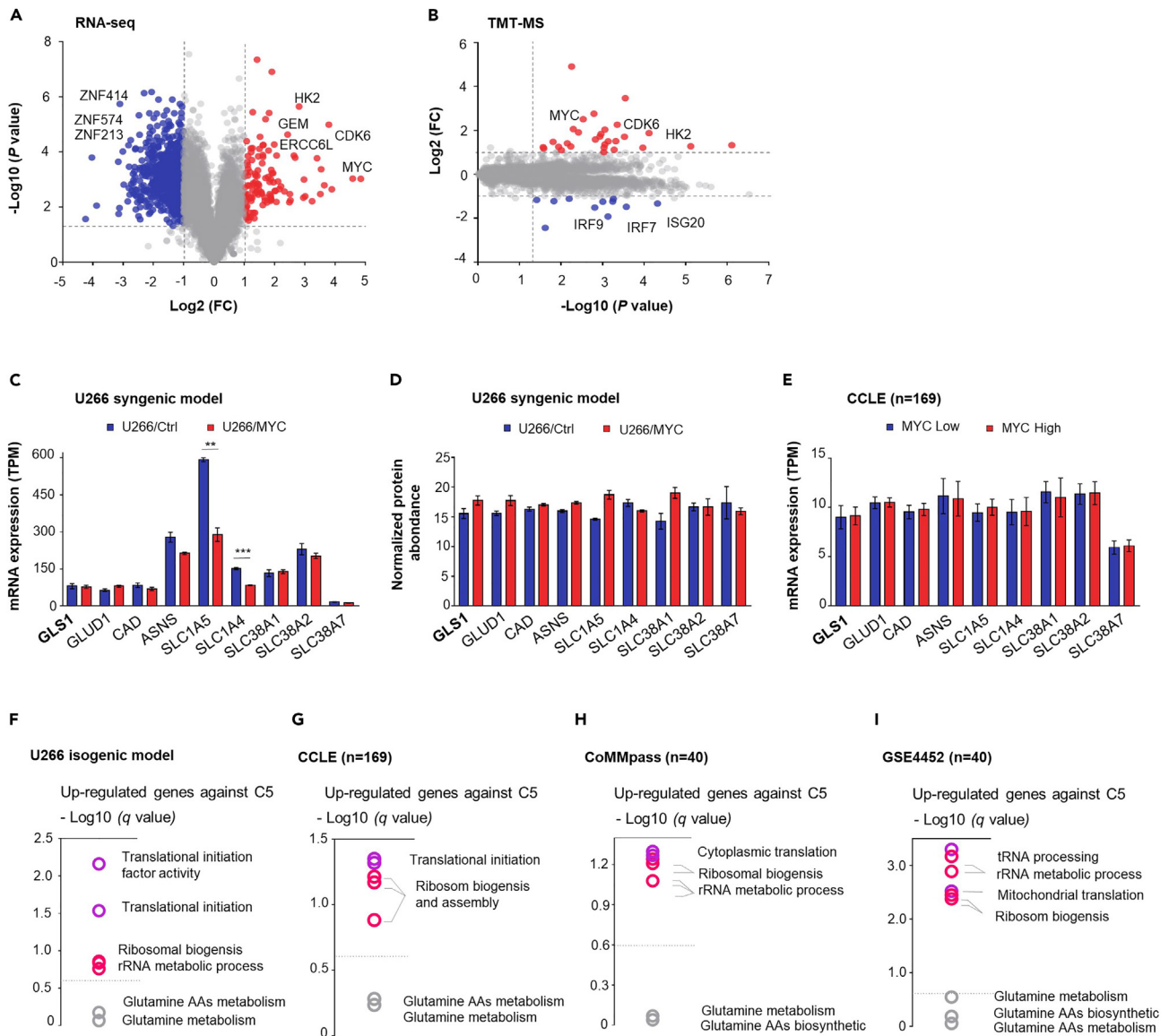


Figure 2. MYC oncogenic signaling and glutamine dependency

(A) Volcano plot of RNA-seq of U266/MYC versus U266/Ctrl showing 119 and 829 genes significantly up-and downregulated, respectively, with a fold change (FC) higher than 2.

(B) Volcano plot of TMT-MS of U266/MYC versus U266/Ctrl showing 28 and 15 proteins significantly up-and downregulated, respectively, with a fold change (FC) higher than 2.

(C) mRNA expression level and D. protein abundance of glutaminolysis-related genes in U266/Ctrl and U266/MYC. Data in (C-D) are represented as mean \pm SEM of triplicates.

(E) Expression data of glutaminolysis-related genes in Hem cell lines (n = 169) from CCLE database (Affymetrix U133 + 2 expression array) grouped into MYC-high versus MYC-low cell lines.

(F-I) Gene set enrichment analysis demonstrating the most significantly up-regulated genes in the context of high MYC expression against C5 gene set, in; F. The U266 isogenic model.

(G) Hem cell lines (n = 169) from CCLE database grouped into MYC-high versus MYC-low cell lines.

(H and I) The cohort of patient datasets: GSE4452 (Carrasco; n = 40), and MMRF RG (CoMMpass; n = 40). Selected pathways were shown. * Indicates p values <0.05, ** indicates p value <0.01, *** indicates p value <0.001; Student's t test.

U266/Ctrl and U266/MYC by running a mitochondrial stress test (Figures 3B and S2A). Both knockdown of GLS1 expression and pharmacologic GLS1 inhibition by CB-839 in U266/MYC was accompanied by mitochondrial impairment at basal and the FCCP-induced (maximal) OCR confers impaired mitochondrial function and consequently reduction in the OXPHOS activity (Figures 3C, 3D, and S2A). The effect of CB-839

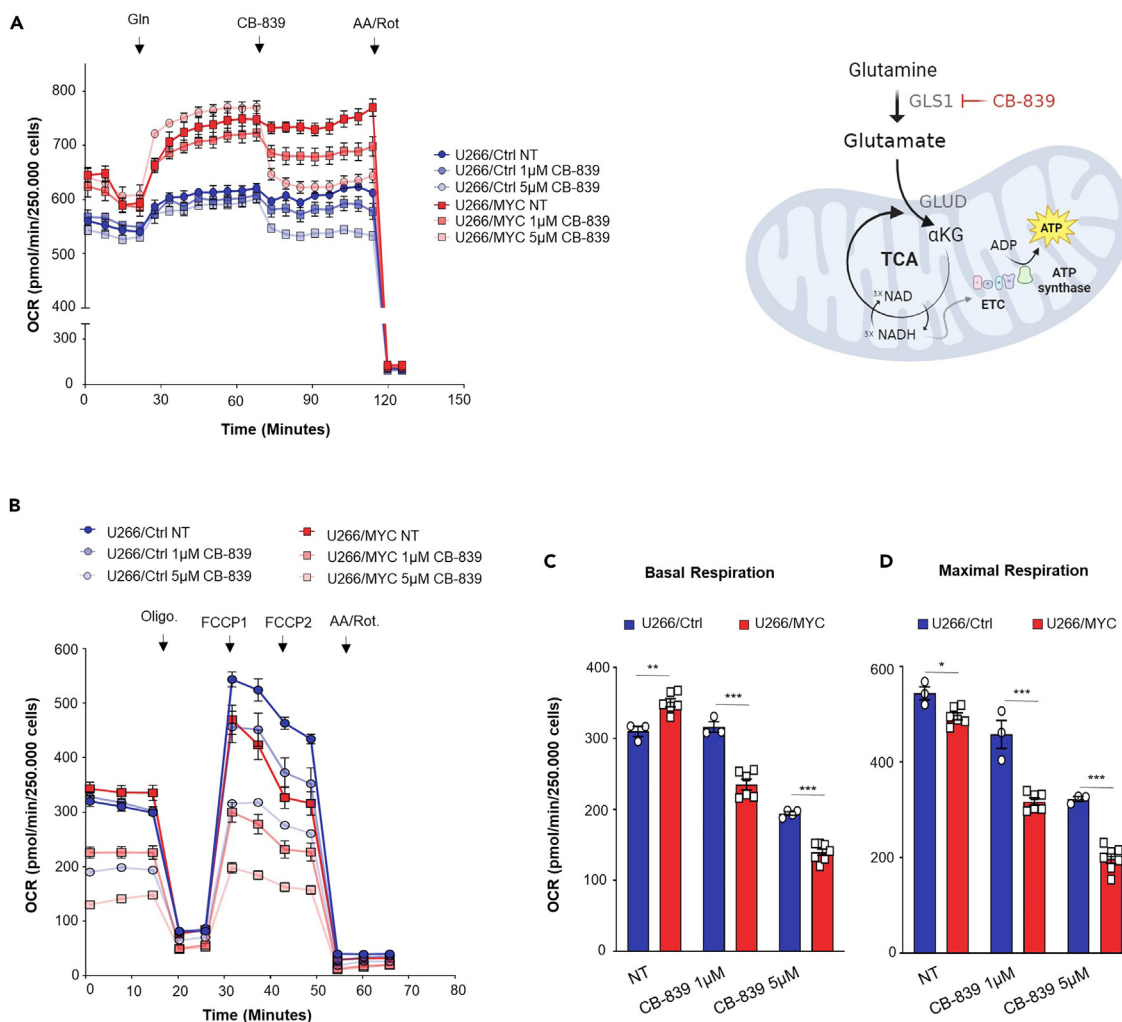


Figure 3. The role of glutamine in maintaining mitochondrial function

(A) Kinetic OCR response in U266/Ctrl and U266/MYC cells to glutamine (2mM) followed by CB-839 at (1 or 5 μ M).

(B) Kinetic plot and corresponding bar graphs of normalized OCR obtained during mitochondrial stress test of U266/Ctrl and U266/MYC treated with or without the indicated concentration of CB-839 for 4 h, cells were exposed sequentially to each mitochondrial modulator of mitochondrial activity at the indicated times to assess.

(C) Basal respiration.

(D) Maximal respiration. Data are presented as mean \pm SEM calculated from 3 technical replicates. * Indicates p values <0.05, ** indicates p value <0.01, *** indicates p value <0.001; Student's t test. DMSO-treated cells were used as a non-treated control (NT).

was observed in dose-dependent manner in U266/MYC, while we observed less impact on U266/Ctrl and only at higher concentration of CB-839. To extend this observation, we generated a second isogenic model overexpressing MYC in Loucy cell line; an acute lymphoblastic leukemia (ALL) cell line that has low MYC expression level. We transduced Loucy cells with EF1A-C-MYC lentiviral vector (Figure S2B). Next, we assessed the metabolic profile of the Loucy isogenic model and observed similar results to the U266 isogenic model. Loucy/MYC showed a significantly higher energetic profile compared to Loucy/Ctrl represented by higher basal and maximal OCR levels. This higher mitochondrial function was impaired by 5 μ M CB-839 (Figures S2C–S2E). Due to the tight link between OXPHOS and glycolysis for ATP production, we next analyzed the glycolytic profile of our isogenic models. Increased doses of CB-839 triggered an increase in glycolytic activity to compensate for the OXPHOS deficit in U266 isogenic model. In contrast, we observed a significant decrease in the glycolytic reserve in U266/MYC upon GLS1 inhibition, indicating a disruption of the cellular potentials to increase ATP production through glycolysis to meet energy demand (Figures S3A–S3C). Similarly, inhibiting GLS1 caused more differential effect on Loucy/MYC, demonstrated by an increase in the glycolytic activity and a decrease in the glycolytic reserve upon CB-839 treatment, while no effects were observed on Loucy/Ctrl cells (Figures S3D–S3F). Taken together, these findings revealed the essential role of GLS1 in the MYC OE cells to sustain their mitochondrial function for energy production.

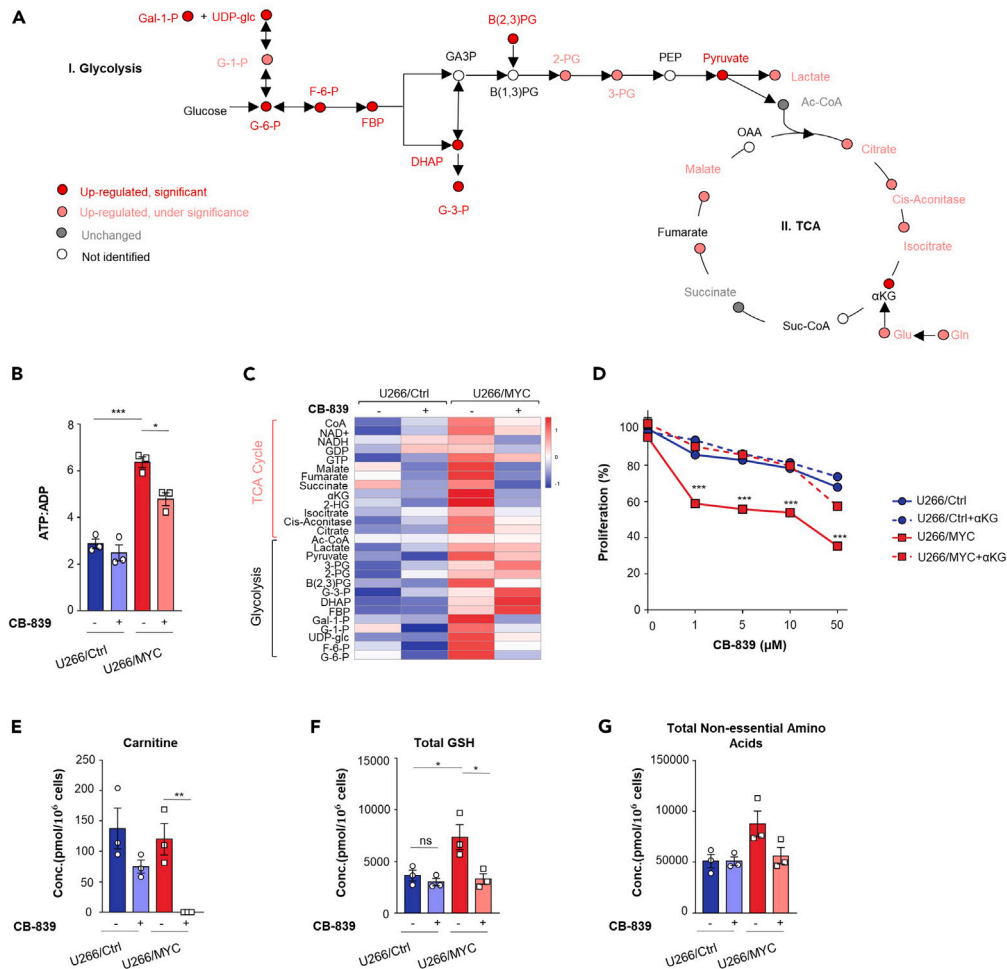


Figure 4. Enriched metabolic pathways under GLS1 inhibition

(A) Shown is a metabolic network of glycolysis and TCA cycle, metabolites abundance was colored by their abundance difference in U266/MYC compared to U266/Ctrl (color key).

(B) ATP:ADP ratio was determined to assess the energy state of U266/Ctrl and U266/MYC treated with 1 μM CB-39 for 48 h.

(C) Heatmap comparing relative levels of metabolites in U266/Ctrl and U266/MYC treated with 1 μM CB-39 for 48 h.

(D) The differential effect of αKG (1 mM) on the viability of U266/Ctrl and U266/MYC cultured under the indicated concentration of CB-839 for 48 h.

(E) Intracellular carnitine (F) Total glutathione and (G) Non-essential amino acids levels, sum of [Ala], [Arg], [Asn], [Asp], [Gln], [Glu], [Gly], [Pro], [Ser] and [Tyr], measured in U266/ctrl and U266/MYC treated with CB-839 for 48 h. All data were normalized to cell count and presented as mean ± SEM of 3 technical replicates. Comparison of more than three groups were performed by one-way ANOVA test. * Indicates p values <0.05, ** indicates p value <0.01, *** indicates p value <0.001. DMSO-treated cells were used as a non-treated control (NT).

CB-839 selective effect is driven by a decreased glutamine utilization in the context of MYC OE

To further determine the downstream effects of GLS1 inhibition in the context of high MYC expression, we analyzed the abundance of 116 key metabolites in U266/MYC and U266/Ctrl cell lines (Table S6). U266/MYC showed a higher glycolytic profile combined with elevated TCA cycle metabolites (Figure 4A). We next identified the metabolic changes under GLS1 inhibition. CB-839 showed a significant reduction in the ATP:ADP ratio in U266/MYC and not U266/Ctrl marking an important energy debt (Figure 4B). Moreover, we found that CB-839 caused significant suppression of the TCA cycle in MYC high cells (Figure 4C). Accordingly, the co-incubation with the main glutamine derivative (αKG) rescued the proliferation defect caused by CB-839 in U266/MYC (Figure 4D). We have also found a significant depletion in the carnitine level under GLS1 inhibition in U266/MYC; thus, the cells failed to accelerate the fatty acid oxidation (FAO) to rescue the resulting energy depletion (Figure 4E). Besides its role as a carbon donor, the resulting glutamate is an indispensable donor of nitrogen for macromolecule synthesis such as glutathione (GSH). GSH has a major role in mitigating the effects of reactive oxygen species (ROS). Notably we observed a significant increase in the total GSH level in U266/MYC. This observation is in line with other studies that linked MYC expression and GSH level.^{21,22} This level was reduced by 54.92 ± 12.1% under GLS1 inhibition (Figure 4F). Furthermore, we observed elevated levels of nonessential amino acids in U266/MYC which indicates a higher translational activity of MYC OE cells, whereas a depletion was observed under GLS1 inhibition

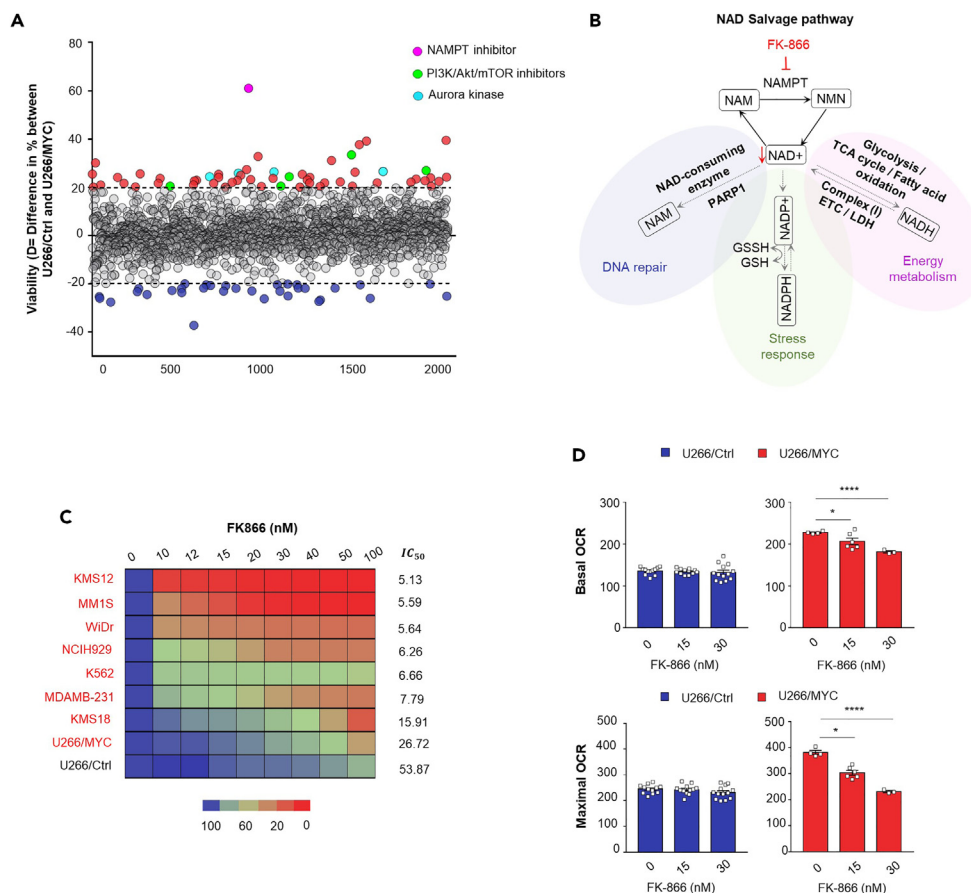


Figure 5. Differential effect of NAMPT inhibition in MYC OE cells

(A) Scatterplot representation of a small-molecule library (~2000 compounds) against U266 isogenic model cells. Each dot represents the inhibition difference between U266/Ctrl and U266/MYC achieved with each compound at a concentration of 10 μ M for 48 h. Hit thresholds were set to >20 (red) or < -20 (blue). Leads were highlighted.

(B) Schematic of the NAD⁺ salvage production pathway and the site of action of NAMPT inhibitor (FK-866) and the major downstream cellular functions of NAD⁺. NAM, nicotinamide; NMN, nicotinamide mononucleotide.

(C) Heatmap represents the dose-response effect on KMS12, WiDr, K562, U266/Ctrl and U266/MYC. Cell lines were treated with FK-866 (0-100nM for 72 h). The percentage survival (expressed as percentage of the DMSO-treated control) is visualized in color format according to their values on a linear scale (0%–100%) and row-ranked by IC₅₀ values from lowest to highest. Cell lines with high MYC expression values were highlighted in red.

(D) Normalized basal and maximal OCR obtained during mitochondrial stress test of U266/Ctrl and U266/MYC with or without the indicated concentration of: FK-866 for 48 h. Data are presented as mean \pm SEM calculated from three technical replicates. DMSO-treated cells were used as a non-treated control (NT). Comparison of more than three groups were performed by one-way ANOVA test. * Indicates p values <0.05, ** indicates p value <0.01, *** indicates p value <0.001.

(Figure 4G). The above results conclusively show that MYC overexpression results in a preferential metabolic shift to Gln to satisfy the elevated needs for energy, redox regulation, and protein synthesis substrates.

NAMPT inhibition selectively affects MYC OE cells

To identify pharmaceutical agents with which to perturb the proliferation of MM cells in the context of MYC overexpression, we performed a small-molecule screen on U266/MYC and U266/Ctrl control cell lines. A total of 1869 well-annotated small molecules were tested, including most of Selleck's inhibitors, FDA-approved compounds, chemotherapeutic agents, as well as some natural products. We determined a differential activity (D-score) for each compound. Among the hits that selectively affected MYC OE cells, we identified five compounds that belong to the PI3K/Akt/mTOR signaling pathway (GSK 1059615, OSU-03012, BIO, AZD 2858, AZD 1080), 5 Aurora kinase inhibitors (MLN8054, VX-680, AMG-900, MLN8237, GSK1059615), (Figure 5A; Table S7). This finding can be reasoned to the enhanced dependency of MYC overexpressing cells on PI3K/Akt/mTOR pathway and Aurora kinase to maintain protein translation and cell division, respectively.^{23,24} Interestingly, the nicotinamide phosphoribosyl transferase (NAMPT) inhibitor STF-11884 had the highest selectivity inhibition on MYC OE cells (D = 61.05%) marking our first lead. NAMPT is the rate-limiting enzyme in the nicotinamide adenine dinucleotide (NAD⁺) synthesis. It catalyzes the first step in the biosynthesis of NAD from nicotinamide (NAM), which is essential for energy production.²⁵ NAD role is extended

to other cellular functions, such as DNA repair through the actions of NAD-consuming enzymes such as PARPs and oxidative stress response^{26,27} (Figure 5B). To validate the dependency of MYC OE cells, we used the NAMPT inhibitor FK-866, evaluated in clinical trials (Phase II) for chronic lymphocytic leukemia and cutaneous T cell lymphoma (NCT00435084 and NCT00431912). We observed a significantly higher sensitivity to FK-866 in MYC overexpressing cells (Figures 5C, 5D, and S4A). From these data, we can conclude a potent and differential effect of NAMPT inhibition on MYC OE.

Synergistic activity of CB-839 and FK-866 in MYC OE cells

Considering that Gln and NAD have closely interlinked metabolic networks involving electron transport chain (ETC), TCA and redox regulation,²⁸ we next explored the potential synergy between GLS1 and NAMPT inhibitors. We performed a dose-response matrix to test 9 different combinations of doses ranging from 0 to 20 μ M for CB839 and from 0 to 30 nM for FK-866. As hypothesized, FK866 markedly enhanced the anti-multiple myeloma effects of CB-839. The dual inhibition of GLS1 and NAMPT showed a synergistic effect in U266/MYC (ZIP synergy score: 35.896 ± 3.78) or MM1S (ZIP synergy score: 22.3612 ± 11.42), (Figure 6A). In contrast, the combined treatment of CB-839 and FK-866 was mostly additive in U266/Ctrl cells (ZIP synergy score: 4.657 ± 8.29). The lowest combinatorial treatment doses tested achieved on average 37–70% more killing in U266/MYC compared to control cells. These data suggest a selective synergy CB-839 and FK-866 in the context of MYC overexpression in MM. This combination caused a reduction at both basal and maximal respiration of 60–40%, respectively (Figures 6B and 6C). Likewise, combining GLS1 and NAMPT1 inhibitors induced the level of mitochondrial oxygen species and led to a significant mitochondrial depolarization in U266/MYC compared to the effect observed in control cells (Figures 6D and 6E). We next assessed the *in vitro* activity of CB-839 and FK-866 against human peripheral blood mono-nuclear cells (PBMCs). Besides significant synergistic cytotoxicity in U266/MYC, the drug combination showed strong selectivity, as survival of healthy PBMCs was dramatically higher (Figure S4B). Taken into consideration the role of NAD supply to maintain the activity of the glycolytic enzyme glyceraldehyde 3-phosphate dehydrogenase (GAPDH), we next set out to measure the glycolytic rate under CB-839 and FK-866 combinatorial treatment. FK-866 effects on the glycolytic rate were observed only after 48 h of incubation on U266/MYC, while no additional effect was observed by adding CB-839. In comparison, no significant effect was observed on U266/Ctrl (Figures S4C and S4D). Moreover, we investigated if the CB-839 and FK-866 combination affects the drug resistance profile of myeloma cells. We used the dexamethasone-resistant MM cell line (MM1R). Potently, increased doses of the combination had cytotoxic effect on the MM1R cell line (Figure S5A). Next, we have tested the two proteasome inhibitors that are considered the cornerstone agents in the treatment of MM, Carfilzomib and Bortezomib in increased doses with increased doses of the CB-839 and FK-866 combination. Effectively our combination improved the sensitivity profile of U266/MYC and MM1S to Carfilzomib and Bortezomib. This effect was less potent in U266/Ctrl cells (Figures S5B–S5G). Our results align with prior investigations that reported PI sensitizing activity of CB-839 in resistant MM cells.²⁹ We further assessed the potential synergy of CB-839 and FK-866 *in vivo*. SCID mice were injected with MM1S GFP-Luc⁺ (Figure 7A). After engraftment, mice were randomized into four groups to receive vehicle, CB-839 (200 mg/kg), FK-866 (10 mg/kg) or a combination of both drugs. We observed that the combination of both metabolic inhibitors elicited a strong anti-tumor activity compared to single-CB-839 treatment, as monitored by bioluminescence (BLI) and prolonged overall survival (OS) median of 38 days for the control group, 42 days and 54.5 for single treatment with CB-839 and FK866, respectively and 64.5 days for combination; $p < 0.0001$ (Figures 7B and 7C). Taken together, our data indicate that the dual inhibition of GLS1 and NAMPT represents an innovative new therapeutic approach to target gene dependencies in MYC overexpressing MM.

DISCUSSION

Despite the role of MYC overexpression in the progression from precursor stages to symptomatic MM, MYC remains a long-pursued target due to the short half-life of the protein, the intrinsically disordered location of its main functional domains, the lack of an enzymatically active site, and its nuclear localization.³⁰ Some strategies to target MYC on different axes, such as transcription, translation, and Myc protein stability or interactions have been studied.^{4,12,31–36} However, despite the massive efforts, targeting MYC on a clinical level remains challenging. Consequently, indirect strategies for targeting MYC have arisen as an important approach to effectively and selectively target MYC-driven cancer cells.

Here, we report for the first time a differential gene dependency of MYC overexpression on GLS1, an enzyme responsible for converting glutamine to glutamate. Glutamate is then subsequently converted to α -ketoglutarate which feeds into the TCA cycle for ATP production. Previous studies have shown that nutrient such as glutamine can modulate MYC post-transcriptionally.³⁷ Moreover, MYC interferes with the expression of GLS1 through inhibiting miR-23a/b thus increases the glutamine utilization.^{38,39} Here, in the context of MM and hematological malignancies, we did not observe an enrichment in the glutamine metabolism pathways in MYC overexpressing cells. This likely reflects that MYC does not induce an overexpression of the glutamine metabolism pathway but is rather dependent on minimal glutaminolysis activity. This suggests a non-oncogenic dependency on GLS1 driven by MYC expression.

We functionally explored these dependencies as a selective targetable vulnerability using CB-839, a potent and selective GLS1 inhibitor currently being used in phase I/II clinical trials in different cancer types (NCT02071927, NCT04250545, NCT03163667). CB-839 exhibited promising preclinical data in several types of solid cancers, such as triple negative cancer,⁴⁰ lung adenocarcinoma,⁴¹ and hematological malignancies, including acute myeloid leukemia (AML).^{42,43} This sensitivity to glutamine inhibition was driven by both redox and bioenergetics stress. In our present study, we demonstrated through different approaches that MYC overexpressing cells exhibit heightened sensitivity to perturbation of glutamine metabolism. Our metabolic assays substantiate the essential role of glutamine in maintaining mitochondrial OXPHOS in MYC overexpressing cells. OXPHOS is an important process that harvests the TCA-generated NADH (nicotinamide adenine dinucleotide) and FADH2

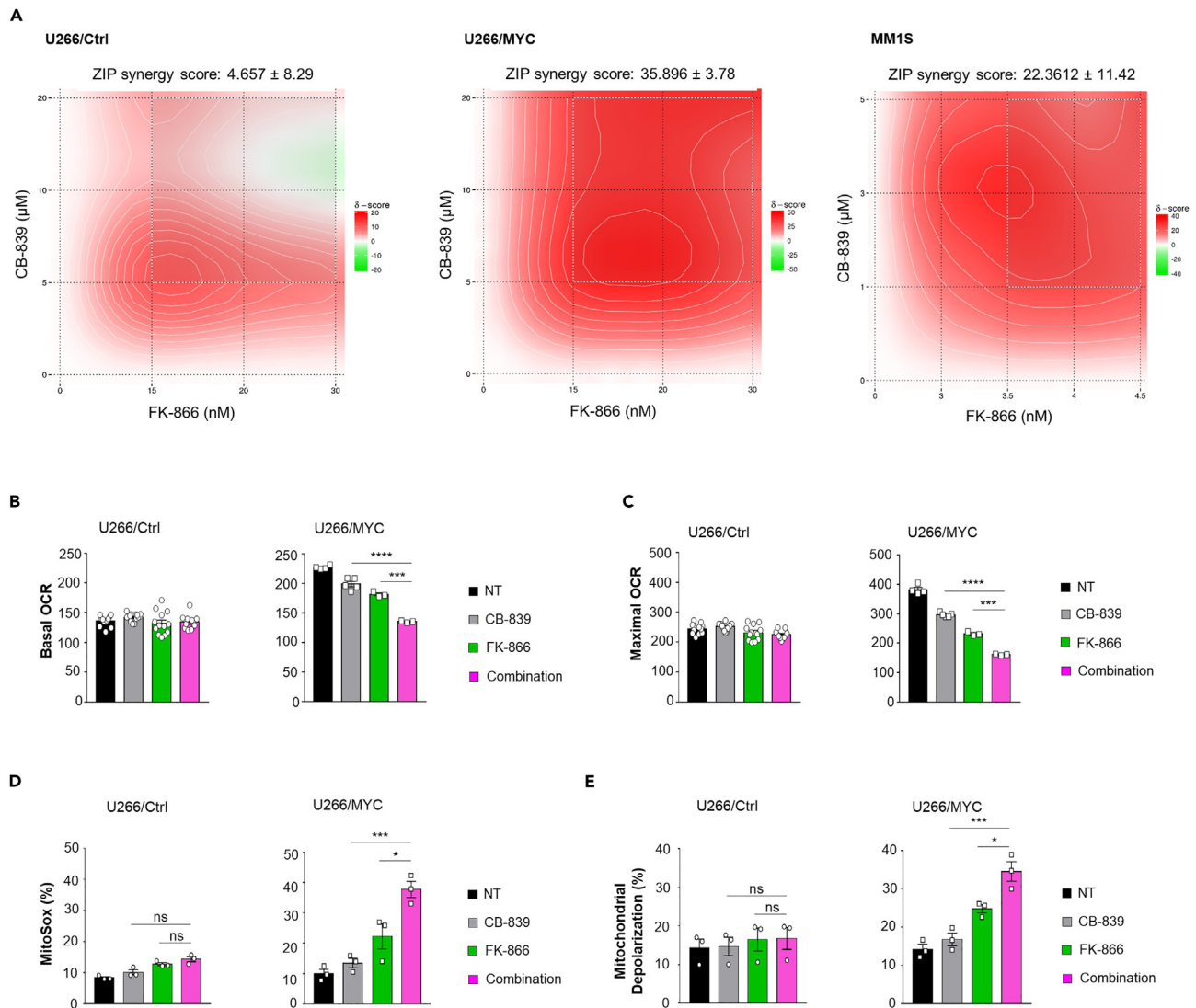


Figure 6. Combining CB-839 and FK-866 is a powerful strategy against MM

(A) Synergy maps of U266/Ctrl, U266/MYC and MM1S cell lines treated with indicated concentration of CB-839 and FK-866 for 72 h. Synergy score was determined by SynergyFinder using zero interaction potency ZIP (N = 3 biologically independent replicates).

(B and C) Normalized Basal and Maximal OCR obtained during mitochondrial stress test of U266/Ctrl and U266/MYC with or without the indicated concentration of: CB-839 (1 μ M) for 4 h, FK-866 (30 nM) for 48 h and combined treatment. Data are presented as mean \pm SEM calculated from 3 technical replicates. DMSO-treated cells were used as a non-treated control (NT).

(D) Mitochondrial superoxide (MitoSOX) and (E) tetramethylrhodamine, ethyl ester (TMRE) evaluated in U266/Ctrl and U266/MYC cells. Cells were treated with FK866 (30 nM) for 72 h and/or CB-839 (5 μ M) for 24 h. Data represent the mean \pm SEM of triplicates of three representative experiments. Comparison of more than three groups were performed by one-way ANOVA test. * Indicates p values <0.05, ** indicates p value <0.01, *** indicates p value <0.001.

(flavine adenine dinucleotide) to produce ATP. Additionally, integrative analyses of metabolomic profiles revealed that MYC overexpression renders MM cells specifically dependent on glutamine to fuel the TCA cycle and maintain high energy production. This observation is in line with previous studies, which reported the important role of glutamine during MM tumorigenesis and an increase in glutamine anaplerosis into the TCA cycle in MM stages compared to pre-malignant stages.^{44,45} Prior studies reported a link between cysteine plasma level and sensitivity to GLS1 inhibitors. The increase in cysteine levels was found to increase the intracellular glutamine turnover, which in turn render the cells more sensitive to glutaminolysis inhibitors such as CB-839. It is worth noting that our CE-MS analysis we did not notice any changes in the cysteine level between our U266/Ctrl cells and U266/MYC.⁴⁶ Besides energy stress, GLS1 inhibition triggers redox stress and causes a reduction of 60% of the antioxidant glutathione level. This result is in agreement with previous studies in various cancer types.^{47,48}

Combining CB-839 with other compounds such as mTOR and checkpoint inhibitors held the promise of synergistic effect to enhance the therapeutic activity.^{49,50} Thus, we investigated potential synergistic combinations that can exacerbate this metabolic vulnerability. Herein, we

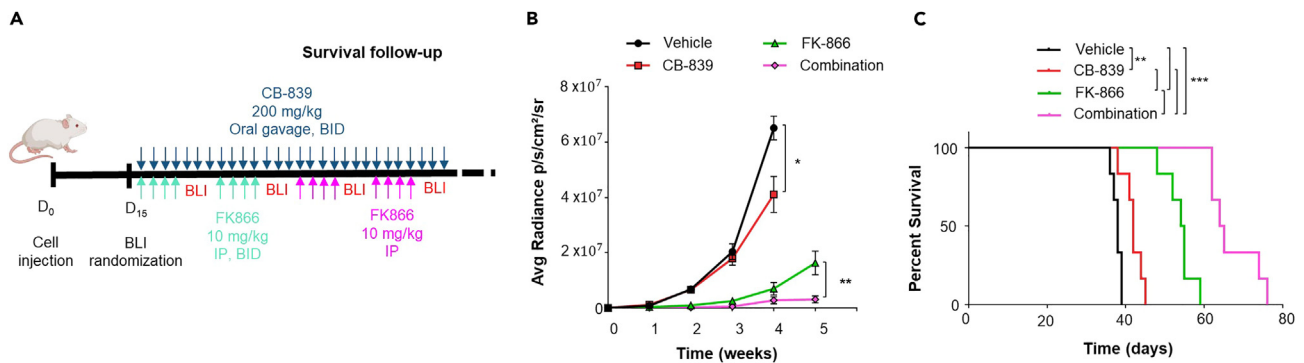


Figure 7. In vivo synergistic effect of combining CB-839 and FK-866

(A) Experimental workflow for the *in vivo* experiments. Female SCID/CB.17 mice were injected with MM.1S-GFP-Luc+ cells. After engraftment mice were randomized to four groups based on bioluminescence (BLI), and CB-839, FK-866, combination or vehicle control was administered. Tumor growth was assessed by BLI at the indicated times.

(B) BLI signal versus time of the four groups of Female SCID/CB.17 mice bearing MM.1S-GFP-Luc+ tumor treated with CB-839, FK-866, combinations, and vehicle control (n = 6). Data are presented as mean \pm SEM.

(C) Kaplan-Meier survival curve, survival was evaluated from the first day of engraftment until mice were sacrificed. * Indicates p values <0.05, ** indicates p value <0.01, *** indicates p value <0.001.

demonstrate a pharmacological dependency of MYC-driven cells on NAMPT. FK866 (also known as APO866) is a highly selective non-competitive NAMPT inhibitor firstly presented in 2003 as the first specific nanomolar inhibitor of NAMPT.⁵¹ Preclinically, FK866 exerts potent antitumor activity on various tumor models.^{52–54} NAMPT inhibition compromises several cellular processes by depleting NAD levels. NAD is a substrate to numerous enzymes such as sirtuins, and ADP-ribosyl, but most importantly, poly (ADP-ribose) polymerase 1 (PARP1), essential for DNA repair therefore crucial to tumors with high genomic instability.⁵⁵ In addition, NAD is a critical cofactor in operating the TCA cycle and glycolysis through oscillating between two redox states (NAD and NADH). Tan et al. showed that FK866 results in the accumulation of glycolytic intermediates and markedly decreases the ATP level.⁵⁶ Here we report a selective potency of FK866 in MYC-driven MM to maintain tumor high energy demands through mitochondrial OXPHOS and not glycolysis.

Due to the tight link between glutamine and NAD biological roles, we examined a novel potential combination between GLS1 and NAMPT1 inhibitors. We observed an exclusive synergy of CB839 and FK866 in MYC overexpressing cells. Collectively, our *in vitro* and *in vivo* results revealed an effective therapeutic combinatory strategy in the context of MYC overexpressing MM. Both drugs are currently used in clinical trials indicating a high translational potential. However, some clinical trials testing FK-866 reported dose-limiting toxicity including thrombocytopenia and gastrointestinal symptoms, thus, we thought of using FK-866 as a complement agent to enhance the efficacy and improve tolerability.

In conclusion, our research was marked by applying both dependency maps and drug screens as a powerful approach to identifying therapeutic candidates in specific molecular subsets of MM with a high translational potential. Here, we highlight a combined approach by interfering with glutamine metabolism and NAD production, and we uncover for the first time a potent synergy between the two metabolic inhibitors, CB-839 and FK-866. Our research opens up the opportunity to repurpose the use of FK866 to overcome its dose-limiting toxicity and to improve the anti-myeloma activity of CB-839 through the co-administration of both metabolic inhibitors. This powerful combination of two clinically tested compounds paves the road to translating preclinical findings into potential clinical applications. The results of this study will need further validation in different models to be potentially translated in the clinic. Moreover, this approach can be extended to identify other potential synergistic partners as novel strategies to target the undruggable MYC-driven tumor cells.

Limitations of the study

One of the limitations of this study was the unavailability of a MM cell line that has low MYC expression levels apart from U266 cell line. While it is theoretically possible to knockdown MYC expression in cell lines to establish two distinct comparison groups within MM, previous studies have reported cytotoxicity associated with such manipulations in myeloma cell lines. However, to address this limitation, we generated two isogenic models overexpressing MYC in myeloma and lymphoma. We have also used an array of cell lines derived from diverse cancer types. Additionally, our study relied on publicly available datasets of expression profiles from both cell lines and patients to further strengthen and validate our conclusions. The other limitation is the lack of another mouse model in which we can further validate this synergy within an immunocompetent environment. Further studies are required to underline the mechanism of this therapeutic synergy *in vivo*.

STAR★METHODS

Detailed methods are provided in the online version of this paper and include the following:

- KEY RESOURCES TABLE
- RESOURCE AVAILABILITY

- Lead contact
- Materials availability
- Data and code availability
- **EXPERIMENTAL MODEL AND STUDY PARTICIPANT DETAILS**
 - Cell culture
 - Mice
 - Human participants
- **METHOD DETAILS**
 - Small-molecule screen
 - Cell viability assay
 - Protein and RNA isolation
 - Western blot analysis
 - Seahorse XF assay
 - Mitochondrial superoxide membrane potential ($\Delta\Psi$) measurements
 - CE-MS spectrometry
 - Lentiviral infection and GLS1 knockdown
 - In silico
 - RNA-Sequencing
 - TMT spectrometry
 - *In vivo* study
- **QUANTIFICATION AND STATISTICAL ANALYSIS**

SUPPLEMENTAL INFORMATION

Supplemental information can be found online at <https://doi.org/10.1016/j.isci.2024.109417>.

ACKNOWLEDGMENTS

This work was supported by ARC France Foundation grant. We also acknowledge the support from Contrat de Plan Etat-Région CPER Cancer 2015–2020. We also thank the Flow Core Facility- BICeL/UAR2014-US41 PLBS “Plateformes Lilloises en Biologie et Santé” for the access and technical support.

AUTHOR CONTRIBUTIONS

L.H.B.I., J.K., and S.Ma. conceived and designed the study. L.H.B.I. and W.L. performed experiments. L.H.B.I., L.F., W.L., R.S.P., I.G., J.K., and S.Ma. acquired the data. All authors analyzed and interpreted the data. L.H.B.I. and S.Ma. wrote the manuscript. All authors reviewed, edited, and approved the manuscript.

DECLARATION OF INTERESTS

The authors declare no conflict of interest.

Received: September 25, 2023

Revised: December 26, 2023

Accepted: March 1, 2024

Published: March 4, 2024

REFERENCES

1. Palumbo, A., and Anderson, K. (2011). Multiple Myeloma. *N. Engl. J. Med.* 364, 1046–1060. <https://doi.org/10.1056/NEJMra1011442>.
2. Landgren, O., Kyle, R.A., Pfeiffer, R.M., Katzmann, J.A., Caporaso, N.E., Hayes, R.B., Dispenzieri, A., Kumar, S., Clark, R.J., Baris, D., et al. (2009). Monoclonal gammopathy of undetermined significance (MGUS) consistently precedes multiple myeloma: a prospective study. *Blood* 113, 5412–5417. <https://doi.org/10.1182/blood-2008-12-194241>.
3. Weiss, B.M., Abadie, J., Verma, P., Howard, R.S., and Kuehl, W.M. (2009). A monoclonal gammopathy precedes multiple myeloma in most patients. *Blood* 113, 5418–5422. <https://doi.org/10.1182/blood-2008-12-195008>.
4. Manier, S., Salem, K.Z., Park, J., Landau, D.A., Getz, G., and Ghobrial, I.M. (2017). Genomic complexity of multiple myeloma and its clinical implications. *Nat. Rev. Clin. Oncol.* 14, 100–113. <https://doi.org/10.1038/nrclinonc.2016.122>.
5. Kuehl, W.M., and Bergsagel, P.L. (2002). Multiple myeloma: evolving genetic events and host interactions. *Nat. Rev. Cancer* 2, 175–187. <https://doi.org/10.1038/nrc746>.
6. Chng, W.-J., Huang, G.F., Chung, T.H., Ng, S.B., Gonzalez-Paz, N., Troska-Price, T., Mulligan, G., Chesi, M., Bergsagel, P.L., and Fonseca, R. (2011). Clinical and biological implications of MYC activation: a common difference between MGUS and newly diagnosed multiple myeloma. *Leukemia* 25, 1026–1035. <https://doi.org/10.1038/leu.2011.53>.
7. Hideshima, T., Mitsiades, C., Tonon, G., Richardson, P.G., and Anderson, K.C. (2007). Understanding multiple myeloma pathogenesis in the bone marrow to identify new therapeutic targets. *Nat. Rev. Cancer* 7, 585–598. <https://doi.org/10.1038/nrc2189>.
8. Shou, Y., Martelli, M.L., Gabrea, A., Qi, Y., Brents, L.A., Roschke, A., Dewald, G., Kirsch,

- I.R., Bergsagel, P.L., and Kuehl, W.M. (2000). Diverse karyotypic abnormalities of the c-myc locus associated with c-myc dysregulation and tumor progression in multiple myeloma. *Proc. Natl. Acad. Sci. USA* 97, 228–233. <https://doi.org/10.1073/pnas.97.1.228>.
9. Affer, M., Chesi, M., Chen, W.D.G., Keats, J.J., Demchenko, Y.N., Roschke, A.V., Van Wier, S., Fonseca, R., Bergsagel, P.L., Kuehl, W.M., et al. (2014). Promiscuous MYC locus rearrangements hijack enhancers but mostly super-enhancers to dysregulate MYC expression in multiple myeloma. *Leukemia* 28, 1725–1735. <https://doi.org/10.1038/leu.2014.70>.
 10. Allevalo, M., Bolotin, E., Grossman, M., Mane-Padros, D., Sladek, F.M., and Martinez, E. (2017). Sequence-specific DNA binding by MYC/MAX to low-affinity MYC motifs. *PLoS One* 12, e0180147. <https://doi.org/10.1371/journal.pone.0180147>.
 11. Dang, C.V., O'Donnell, K.A., Zeller, K.I., Nguyen, T., Osthus, R.C., and Li, F. (2006). The c-Myc target gene network. *Semin. Cancer Biol.* 16, 253–264. <https://doi.org/10.1016/j.semcancer.2006.07.014>.
 12. Chen, H., Liu, H., and Qing, G. (2018). Targeting oncogenic Myc as a strategy for cancer treatment. *Signal Transduct. Targeted Ther.* 3, 5. <https://doi.org/10.1038/s41392-018-0008-7>.
 13. Rajagopalan, K.N., and DeBerardinis, R.J. (2011). Role of Glutamine in Cancer: Therapeutic and Imaging Implications: FIGURE 1. *J. Nucl. Med.* 52, 1005–1008. <https://doi.org/10.2967/jnumed.110.084244>.
 14. DeBerardinis, R.J., and Cheng, T. (2010). Q's next: the diverse functions of glutamine in metabolism, cell biology and cancer. *Oncogene* 29, 313–324. <https://doi.org/10.1038/nc.2009.358>.
 15. Revollo, J.R., Grimm, A.A., and Imai, S.i. (2004). The NAD Biosynthesis Pathway Mediated by Nicotinamide Phosphoribosyltransferase Regulates Sir2 Activity in Mammalian Cells. *J. Biol. Chem.* 279, 50754–50763. <https://doi.org/10.1074/jbc.M408388200>.
 16. Liberzon, A., Birger, C., Thorvaldsdóttir, H., Ghandi, M., Mesirov, J.P., and Tamayo, P. (2015). The Molecular Signatures Database Hallmark Gene Set Collection. *Cell Syst.* 1, 417–425. <https://doi.org/10.1016/j.cels.2015.12.004>.
 17. Schlosser, I., Hölzel, M., Mürnseer, M., Burtscher, H., Weidle, U.H., and Eick, D. (2003). A role for c-Myc in the regulation of ribosomal RNA processing. *Nucleic Acids Res.* 31, 6148–6156. <https://doi.org/10.1093/nar/gkg794>.
 18. Van Riggelen, J., Yetil, A., and Felsher, D.W. (2010). MYC as a regulator of ribosome biogenesis and protein synthesis. *Nat. Rev. Cancer* 10, 301–309. <https://doi.org/10.1038/nrc2819>.
 19. Schmidt, E.V. (2004). The role of c-myc in regulation of translation initiation. *Oncogene* 23, 3217–3221. <https://doi.org/10.1038/sj.onc.1207548>.
 20. Manier, S., Huynh, D., Shen, Y.J., Zhou, J., Yusufzai, T., Salem, K.Z., Ebricht, R.Y., Shi, J., Park, J., Glavey, S.V., et al. (2017). Inhibiting the oncogenic translation program is an effective therapeutic strategy in multiple myeloma. *Sci. Transl. Med.* 9, eaal2668. <https://doi.org/10.1126/scitranslmed.aal2668>.
 21. Tambay, V., Raymond, V.-A., and Bilodeau, M. (2021). MYC Rules: Leading Glutamine Metabolism toward a Distinct Cancer Cell Phenotype. *Cancers* 13, 4484. <https://doi.org/10.3390/cancers13174484>.
 22. Lu, S.C. (2009). Regulation of glutathione synthesis. *Mol. Aspect. Med.* 30, 42–59. <https://doi.org/10.1016/j.mam.2008.05.005>.
 23. Yang, D., Liu, H., Goga, A., Kim, S., Yuneva, M., and Bishop, J.M. (2010). Therapeutic potential of a synthetic lethal interaction between the MYC proto-oncogene and inhibition of aurora-B kinase. *Proc. Natl. Acad. Sci. USA* 107, 13836–13841. <https://doi.org/10.1073/pnas.1008366107>.
 24. Pourdehnad, M., Truitt, M.L., Siddiqi, I.N., Ducker, G.S., Shokat, K.M., and Ruggero, D. (2013). Myc and mTOR converge on a common node in protein synthesis control that confers synthetic lethality in Myc-driven cancers. *Proc. Natl. Acad. Sci. USA* 110, 11988–11993. <https://doi.org/10.1073/pnas.1310230110>.
 25. Stein, L.R., and Imai, S.i. (2012). The dynamic regulation of NAD metabolism in mitochondria. *Trends Endocrinol. Metabol.* 23, 420–428. <https://doi.org/10.1016/j.tem.2012.06.005>.
 26. Garten, A., Schuster, S., Penke, M., Gorski, T., de Giorgis, T., and Kiess, W. (2015). Physiological and pathophysiological roles of NAMPT and NAD metabolism. *Nat. Rev. Endocrinol.* 11, 535–546. <https://doi.org/10.1038/nrendo.2015.117>.
 27. Hong, S.M., Park, C.W., Kim, S.W., Nam, Y.J., Yu, J.H., Shin, J.H., Yun, C.H., Im, S.-H., Kim, K.-T., Sung, Y.C., and Choi, K.Y. (2016). NAMPT suppresses glucose deprivation-induced oxidative stress by decreasing NADPH levels in breast cancer. *Oncogene* 35, 3544–3554. <https://doi.org/10.1038/nc.2015.415>.
 28. Heske, C.M. (2019). Beyond Energy Metabolism: Exploiting the Additional Roles of NAMPT for Cancer Therapy. *Front. Oncol.* 9, 1514. <https://doi.org/10.3389/fonc.2019.01514>.
 29. Thompson, R.M., Dytfield, D., Reyes, L., Robinson, R.M., Smith, B., Manevich, Y., Jakubowiak, A., Komarnicki, M., Przybyłowicz-Chalecka, A., Szczepaniak, T., et al. (2017). Glutaminase inhibitor CB-839 synergizes with carfilzomib in resistant multiple myeloma cells. *Oncotarget* 8, 35863–35876. <https://doi.org/10.18632/oncotarget.16262>.
 30. Llobart, V., and Mansour, M.R. (2022). Therapeutic targeting of “undruggable” MYC. *EBioMedicine* 75, 103756. <https://doi.org/10.1016/j.ebiom.2021.103756>.
 31. Allen-Petersen, B.L., and Sears, R.C. (2019). Mission Possible: Advances in MYC Therapeutic Targeting in Cancer. *BioDrugs* 33, 539–553. <https://doi.org/10.1007/s40259-019-00370-5>.
 32. Ba, M., Long, H., Yan, Z., Wang, S., Wu, Y., Tu, Y., Gong, Y., and Cui, S. (2018). BRD4 promotes gastric cancer progression through the transcriptional and epigenetic regulation of c-MYC. *J. Cell. Biochem.* 119, 973–982. <https://doi.org/10.1002/jcb.26264>.
 33. Constantin, T.A., Greenland, K.K., Varela-Carver, A., and Bevan, C.L. (2022). Transcription associated cyclin-dependent kinases as therapeutic targets for prostate cancer. *Oncogene* 41, 3303–3315. <https://doi.org/10.1038/s41388-022-02347-1>.
 34. Viswanathan, S.R., Powers, J.T., Einhorn, W., Hoshida, Y., Ng, T.L., Toffanin, S., O'Sullivan, M., Lu, J., Phillips, L.A., Lockhart, V.L., et al. (2009). Lin28 promotes transformation and is associated with advanced human malignancies. *Nat. Genet.* 41, 843–848. <https://doi.org/10.1038/ng.392>.
 35. DeImore, J.E., Issa, G.C., Lemieux, M.E., Rahl, P.B., Shi, J., Jacobs, H.M., Kastiris, E., Gilpatrick, T., Paranal, R.M., Qi, J., et al. (2011). BET Bromodomain Inhibition as a Therapeutic Strategy to Target c-Myc. *Cell* 146, 904–917. <https://doi.org/10.1016/j.cell.2011.08.017>.
 36. Mazur, P.K., Herner, A., Mello, S.S., Wirth, M., Hausmann, S., Sánchez-Rivera, F.J., Lofgren, S.M., Kuschna, T., Hahn, S.A., Vangala, D., et al. (2015). Combined inhibition of BET family proteins and histone deacetylases as a potential epigenetics-based therapy for pancreatic ductal adenocarcinoma. *Nat. Med.* 21, 1163–1171. <https://doi.org/10.1038/nm.3952>.
 37. Effenberger, M., Bommert, K.S., Kunz, V., Kruk, J., Leich, E., Rudelius, M., Bargou, R., and Bommert, K. (2017). Glutaminase inhibition in multiple myeloma induces apoptosis via MYC degradation. *Oncotarget* 8, 85858–85867. <https://doi.org/10.18632/oncotarget.20691>.
 38. Wise, D.R., DeBerardinis, R.J., Mancuso, A., Sayed, N., Zhang, X.-Y., Pfeiffer, H.K., Nissim, I., Daikhin, E., Yudkoff, M., McMahon, S.B., and Thompson, C.B. (2008). Myc regulates a transcriptional program that stimulates mitochondrial glutaminolysis and leads to glutamine addiction. *Proc. Natl. Acad. Sci. USA* 105, 18782–18787. <https://doi.org/10.1073/pnas.0810199105>.
 39. Gao, P., Tchernyshyov, I., Chang, T.-C., Lee, Y.-S., Kita, K., Ochi, T., Zeller, K.I., De Marzo, A.M., Van Eyk, J.E., Mendell, J.T., and Dang, C.V. (2009). c-Myc suppression of miR-23a/b enhances mitochondrial glutaminase expression and glutamine metabolism. *Nature* 458, 762–765. <https://doi.org/10.1038/nature07823>.
 40. Gross, M.I., Demo, S.D., Dennison, J.B., Chen, L., Chernov-Rogan, T., Goyal, B., Janes, J.R., Laidig, G.J., Lewis, E.R., Li, J., et al. (2014). Antitumor Activity of the Glutaminase Inhibitor CB-839 in Triple-Negative Breast Cancer. *Mol. Cancer Therapeut.* 13, 890–901. <https://doi.org/10.1158/1535-7163.MCT-13-0870>.
 41. Galan-Cobo, A., Sittithideatphaiboon, P., Qu, X., Poteete, A., Pisegna, M.A., Tong, P., Chen, P.-H., Boroughs, L.K., Rodriguez, M.L.M., Zhang, W., et al. (2019). LKB1 and KEAP1/NRF2 Pathways Cooperatively Promote Metabolic Reprogramming with Enhanced Glutamine Dependence in KRAS-Mutant Lung Adenocarcinoma. *Cancer Res.* 79, 3251–3267. <https://doi.org/10.1158/0008-5472.CAN-18-3527>.
 42. Jacque, N., Ronchetti, A.M., Larrue, C., Meunier, G., Birsén, R., Willems, L., Saland, E., Decroocq, J., Maciel, T.T., Lambert, M., et al. (2015). Targeting glutaminolysis has antileukemic activity in acute myeloid leukemia and synergizes with BCL-2 inhibition. *Blood* 126, 1346–1356. <https://doi.org/10.1182/blood-2015-01-621870>.
 43. Matre, P., Velez, J., Jacamo, R., Qi, Y., Su, X., Cai, T., Chan, S.M., Lodi, A., Sweeney, S.R., Ma, H., et al. (2016). Inhibiting glutaminase in acute myeloid leukemia: metabolic dependency of selected AML subtypes. *Oncotarget* 7, 79722–79735. <https://doi.org/10.18632/oncotarget.12944>.

44. Gonsalves, W.I., Jang, J.S., Jessen, E., Hitosugi, T., Evans, L.A., Jevremovic, D., Petterson, X.-M., Bush, A.G., Gransee, J., Anderson, E.I., et al. (2020). In vivo assessment of glutamine anaplerosis into the TCA cycle in human pre-malignant and malignant clonal plasma cells. *Cancer Metabol.* **8**, 29. <https://doi.org/10.1186/s40170-020-00235-4>.
45. Bolzoni, M., Chiu, M., Accardi, F., Vescovini, R., Airoldi, I., Storti, P., Todoerti, K., Agnelli, L., Missale, G., Andreoli, R., et al. (2016). Dependence on glutamine uptake and glutamine addiction characterize myeloma cells: a new attractive target. *Blood* **128**, 667–679. <https://doi.org/10.1182/blood-2016-01-690743>.
46. Muir, A., Danai, L.V., Gui, D.Y., Waingarten, C.Y., Lewis, C.A., and Vander Heiden, M.G. (2017). Environmental cystine drives glutamine anaplerosis and sensitizes cancer cells to glutaminase inhibition. *Elife* **6**, e27713. <https://doi.org/10.7554/eLife.27713>.
47. Jin, H., Wang, S., Zaal, E.A., Wang, C., Wu, H., Bosma, A., Jochems, F., Isima, N., Jin, G., Lieftink, C., et al. (2020). A powerful drug combination strategy targeting glutamine addiction for the treatment of human liver cancer. *Elife* **9**, e56749. <https://doi.org/10.7554/eLife.56749>.
48. Sayin, V.I., LeBoeuf, S.E., Singh, S.X., Davidson, S.M., Biancur, D., Guzelhan, B.S., Alvarez, S.W., Wu, W.L., Karakousi, T.R., Zavitsanou, A.M., et al. (2017). Activation of the NRF2 antioxidant program generates an imbalance in central carbon metabolism in cancer. *Elife* **6**, e28083. <https://doi.org/10.7554/eLife.28083>.
49. Varghese, S., Pramanik, S., Williams, L.J., Hodges, H.R., Hudgens, C.W., Fischer, G.M., Luo, C.K., Knighton, B., Tan, L., Lorenzi, P.L., et al. (2021). The Glutaminase Inhibitor CB-839 (Telaglenastat) Enhances the Antimelanoma Activity of T-Cell-Mediated Immunotherapies. *Mol. Cancer Therapeut.* **20**, 500–511. <https://doi.org/10.1158/1535-7163.MCT-20-0430>.
50. Momcilovic, M., Bailey, S.T., Lee, J.T., Fishbein, M.C., Braas, D., Go, J., Graeber, T.G., Parlati, F., Demo, S., Li, R., et al. (2018). The GSK3 Signaling Axis Regulates Adaptive Glutamine Metabolism in Lung Squamous Cell Carcinoma. *Cancer Cell* **33**, 905–921.e5. <https://doi.org/10.1016/j.ccell.2018.04.002>.
51. Hasmann, M., and Schemainda, I. (2003). **FK866, a highly specific noncompetitive inhibitor of nicotinamide phosphoribosyltransferase, represents a novel mechanism for induction of tumor cell apoptosis.** *Cancer Res.* **63**, 7436–7442.
52. Nahimana, A., Attinger, A., Aubry, D., Greaney, P., Ireson, C., Thougard, A.V., Tjørnelund, J., Dawson, K.M., Dupuis, M., and Duchosal, M.A. (2009). The NAD biosynthesis inhibitor APO866 has potent antitumor activity against hematologic malignancies. *Blood* **113**, 3276–3286. <https://doi.org/10.1182/blood-2008-08-173369>.
53. Olesen, U.H., Thougard, A.V., Jensen, P.B., and Sehested, M. (2010). A Preclinical Study on the Rescue of Normal Tissue by Nicotinic Acid in High-Dose Treatment with APO866, a Specific Nicotinamide Phosphoribosyltransferase Inhibitor. *Mol. Cancer Therapeut.* **9**, 1609–1617. <https://doi.org/10.1158/1535-7163.MCT-09-1130>.
54. Billington, R.A., Genazzani, A.A., Travelli, C., and Condorelli, F. (2008). NAD depletion by FK866 induces autophagy. *Autophagy* **4**, 385–387. <https://doi.org/10.4161/auto.5635>.
55. Pogrebniak, A., Schemainda, I., Azzam, K., Pelka-Fleischer, R., Nüssler, V., and Hasmann, M. (2006). Chemopotentiating effects of a novel nad biosynthesis inhibitor, fk866, in combination with antineoplastic agents. *Eur. J. Med. Res.* **11**, 313–321.
56. Tan, B., Young, D.A., Lu, Z.-H., Wang, T., Meier, T.I., Shepard, R.L., Roth, K., Zhai, Y., Huss, K., Kuo, M.-S., et al. (2013). Pharmacological Inhibition of Nicotinamide Phosphoribosyltransferase (NAMPT), an Enzyme Essential for NAD+ Biosynthesis, in Human Cancer Cells. *J. Biol. Chem.* **288**, 3500–3511. <https://doi.org/10.1074/jbc.M112.394510>.

STAR★METHODS

KEY RESOURCES TABLE

REAGENT or RESOURCE	SOURCE	IDENTIFIER
Antibodies		
anti-c-MYC	Cell Signaling Technology	Cat. # 9402s; RRID: AB_2151827
anti-GLS1	Cell Signaling Technology	Cat. # 88964; RRID: AB_2800133
anti-GAPDH	Santa Cruz Biotechnology	Cat. # sc-47724; RRID: AB_627678
IgG HRP-linked; anti-rabbit	Cell Signaling Technology	Cat. # 7074s; RRID: AB_2099233
IgG HRP-linked; anti-mouse	Cell Signaling Technology	Cat. # 7076s; RRID: AB_330924
Bacterial and virus strains		
EF1A-C-MYC lentivirus	Cellomics Technology	PLV-10010-50
EF1A-Vector Control lentivirus	Cellomics Technology	PLV-10074-50
Chemicals, peptides, and recombinant proteins		
CB-839	MedChemExpress	HY-12248
FK866	MedChemExpress	HY-50876
FCCP	Sigma	C2920
Oligomycin A	Sigma	75351
Antimycin A	Sigma	A8674
Rotenone	Sigma	R8875
Poly-L-lysine solution	Sigma	D8375
Glucose	Gibco	A2494001
2-DG	Sigma	D8375-1g
Dimethyl 2-oxoglutarate	Sigma-Aldrich	349631
Doxycycline	MedChemExpress	HY-N0565,
Hygromycin	InvivoGen	ant-hg-1
Puromycin	InvivoGen	ant-pr-1
Polybrene	Santa Cruz Biotechnology	sc-134220
Phosphatase Inhibitor Cocktail C	Santa Cruz Biotechnology	sc-45065
Phosphatase Inhibitor Cocktail B	Santa Cruz Biotechnology	sc-45045
RIPA lysis buffer	Cell Signaling Technology	Cat. # 9806
BSA	Sigma-Aldrich	Cat. # A2153
Iodoacetamide	Sigma	I1149
Dithiothreitol	Thermo Fisher	P2325
Saline	Aguttant	3400936694132
Citrate	Sigma-Aldrich	PHR1416
Hydroxypropyl- β -cyclodextrin	MedChemExpress	HY-101103
Luciferin	PerkinElmer	122799
MitoSox Red	Thermo Fisher	M36008
Critical commercial assays		
CellTiter-Glo®	Promega	G7571
RNeasy Micro Kit	Qiagen	74104
Pierce™ BCA Protein Assay Kit	Thermo scientific	23225
SuperSignal™ West Femto Maximum Sensitivity Substrate	Thermo scientific	34094
NEBNext® Ultra™ RNA Library Prep Kit	New England BioLabs	NEB #E7770

(Continued on next page)

Continued

REAGENT or RESOURCE	SOURCE	IDENTIFIER
TMRE-Mitochondrial Membrane Potential Assay Kit	abcam	ab113852

Deposited data

Data of RNA-seq	This paper	GEO: GSE241948
Proteomics data	This paper	ProteomeXchange: PXD050010

Experimental models: Cell lines

Human: U266	DMSZ	ACC 9
Human: MM1S	ATCC	CRL-2974
Human: KMS-12	DMSZ	ACC 551
Human: Loucy	ATCC	CRL-2629
Human: MM1S.luc/GFP	Gifts from Dr. Ghobrial (Dana-Farber Cancer Institute)	N/A
Human: MM1R	Gifts from Dr. Ghobrial (Dana-Farber Cancer Institute)	N/A
Human: KMS18	Gifts from Dr. Ghobrial (Dana-Farber Cancer Institute)	N/A
Human: NCI-H929	ATCC	CRL-3580
Human: MDAMB-231	ATCC	CRM-HTB-26
Human: Caki-2	ATCC	HTB-47
Human: WiDr	ATCC	CCL-218
Human: NCIH-23	ATCC	CRL-5800
Human: NCIH-1650	ATCC	CRL-5883
Human: NCIH-1473	ATCC	CRL-5872
Human: K562	ATCC	CCL-243

Experimental models: Organisms/strains

Mouse: SCID	Charles River	Strain code: 236
-------------	---------------	------------------

Oligonucleotides

shGLS1-1 (tet,Hyg)	FenicsBIO	HSH-812279-Hyg-2
shGLS1-2 (tet,Hyg)	FenicsBIO	HSH-812279-Hyg-3
shRNA (tet,Hyg)	FenicsBIO	SH-tet-C02

Software and algorithms

GraphPad Prism 7	GraphPad software	N/A
Living Image 2.5	Living Image 2.5	N/A
GSEA 4.3.1	GSEA software	https://www.gsea-msigdb.org/gsea/doc/GSEAUUserGuideFrame.html
SynergyFinder (version 3.0)	Synergy Finder software	https://synergyfinder.fimm.fi/synergy/20230920124710012638/
Wave (version 2.2.0)	XF Software; Agilent	https://www.agilent.com/en/products/cell-analysis/software-download-for-wave-desktop
Kaluza (version 2.2)	Beckman Coulter	https://www.beckman.fr/flowcytometry/software/kaluza/downloads

RESOURCE AVAILABILITY

Lead contact

Further information and requests for resources and reagents should be directed to and will be fulfilled by the lead contact, Salomon Manier (salomon.manier@inserm.fr).

Materials availability

This study did not generate new unique reagents.

Data and code availability

- This paper analyzed existing, publicly available data. These accession numbers and links were listed in [method details](#). The RNA sequencing raw data have been deposited in Gene Expression Omnibus under GEO: GSE241948. The mass spectrometry proteomics data and analyses have been deposited to the ProteomeXchange Consortium via the PRIDE partner repository and are publicly available with the dataset identifier: PXD050010.
- This paper does not report original code.
- Any additional information required to reanalyze the data reported in this work paper is available from the [lead contact](#) upon request.

EXPERIMENTAL MODEL AND STUDY PARTICIPANT DETAILS

Cell culture

All the cells used in this study are of human origin and were cultured in a humidified incubator at 37°C and 5% CO₂ atmosphere. U266, Loucy, KMS-12, MM1S, K562, MDAMB-231, NCIH-23, NCIH-1650 and NCIH-1473 were cultured in RPMI 1640 with GlutaMAX (Gibco, 61870010). Caki-2, WiDr cell lines were cultured in Dulbecco's modified Eagle's medium (DMEM) with GlutaMAX (Gibco, 31966021). Both mediums were supplied with 10% fetal bovine serum and 1% penicillin/streptomycin. For glutamine deprivations, all cell lines were cultured in glutamine-free RPMI (Gibco, 21870076) supplemented with 10% fetal bovine serum and 1% penicillin/streptomycin. MM1S luc/GFP cells were gifts from Dr. Ghobrial (Dana-Farber Cancer Institute) and cultured in RPMI 1640 with GlutaMAX (Gibco, 61870010) supplied with 10% fetal bovine serum and 1% penicillin/streptomycin before xenograft.

Mice

Animal experiments were conducted in accordance with the "Ministère de l'enseignement supérieur, de la recherche et de l'innovation" and European Animal Care guidelines (protocol no. 32950-2021060215277693 v9). Female SCID/CB.17 mice (n=6 per group) were obtained from Charles River Laboratories; mice were 6 weeks-old, 17–20 g. Mice were housed 4 per cage, with a 12-hour light/dark cycle and were allowed to access food and water. Mice were allowed to acclimatize for one week prior to the experiment.

Human participants

Human blood samples were collected from healthy adult donors (3 females, mean age 27.6 ± 2.2). Race/ethnicity information for human participants cannot be divulged in accordance with local legal constraints. All participants signed an informed consent obtained in accordance with (Etablissement Français du Sang, PLER/2021/005). Peripheral blood mononuclear cells (PBMCs) of healthy donors were isolated from the peripheral blood of healthy volunteers by density gradient centrifugation using Pancoll human (PAN-Biotech, P04-60500) according to the manufacturer's instructions. Briefly, blood samples were collected into ethylenediaminetetraacetic acid-anticoagulated tubes. An equal volume of PBS was used to dilute the blood sample, underlaid with 15ml Pancoll layer. Afterwards, samples were centrifuged at 400g for 30 min using a swinging bucket rotor without braking or deceleration set to 0. Mononuclear cells were collected into sterile labeled 15ml conical tube and washed twice with PBS. Freshly isolated cells were resuspended in RPMI-1640 containing 1% penicillin/streptomycin and 10% fetal bovine serum (FBS) for further analysis.

METHOD DETAILS

Small-molecule screen

U266/Ctrl and U266/MYC cells were treated with 1902 compounds purchased from Selleck Chemicals provided by ICCB-Longwood screening facility, Harvard Medical School. A microplate dispenser, Multidrop™ Combi (Thermo Fisher Scientific), was used to dispense 5,000 cells per well into 384-well microplates. Compounds were added using Seiko Compound Transfer Robot (SGM 611) (V&P Scientific, Inc., CA, USA) at 1 μM final concentration. 48 hours post-treatment cytotoxicity was measured by CellTiter-Glo® Luminescent Cell Viability Assay (Promega) according to manufacturer's protocol and luminescence signals were read using EnVision (Perkin Elmer) plate reader.

Cell viability assay

Relative cell growth and survival were measured in 96-well microplate format by using CellTiter-Glo® Luminescent Cell Viability Assay or Caspase-Glo (Promega) as the end point. Cells were seeded at a density of 30,000 cells per well for suspension cells, 5,000 cells per well for adherent cells and 200,000 cells per well for PBMCs. Luminescence signals were detected using SpectraMAX. Drug sensitivity was then compared by calculating the IC₅₀ values of used cell lines.

Protein and RNA isolation

Proteins were extracted from 2×10^6 to 3×10^6 cells, cells were pelleted at $300 \times g$ for 5 minutes at room temperature. Pellets were washed with ice cold PBS then lysed using RIPA lysis buffer (Cell Signaling) supplemented with Phosphatase Inhibitor Cocktails (Santa Cruz Biotechnology). Lysates were centrifuged at $12000 \times g$ for 15 minutes at 4°C and supernatant was kept at -80°C for further uses. Total RNA was isolated from cells using RNeasy Micro Kit (Qiagen) according to the manufacturer's instructions and evaluated for quantity and quality by NanoDrop spectrophotometer.

Western blot analysis

Protein concentration was measured using Pierce™ BCA Protein Assay Kit (Thermo Scientific) according to the manufacture protocol. For Western blot $80 \mu\text{g}$ of protein was electrophoresed on and subsequently blotted to nitrocellulose membrane. After blocking with 5% BSA (bovine serum albumin, Sigma-Aldrich) in TBST, blots were incubated with primary antibody overnight and subsequently incubated with secondary antibodies conjugated with horseradish peroxidase (HRP) for one hour. Primary antibody: antibody: anti-c-MYC (1:800), anti-GLS1 (1:800) (Cell Signaling Technology) and anti-GAPDH (1:1000, Santa Cruz). IgG HRP-linked; anti-rabbit (1:3000), anti-mouse (1:3000) (Cell Signaling) Signals were detected using SuperSignal™ West Femto Maximum Sensitivity Substrate (ThermoFisher scientific) and detected with LAS 4000 (GE-Healthcare).

Seahorse XF assay

Oxygen consumption rate and extracellular acidification rate (OCR and ECAR) measurements were performed using the XFe24 or XFe96 Extracellular Flux analyzer (Seahorse Bioscience, Billerica, MA, USA) with standard 24-well or 96-well Seahorse microplates. Briefly, XFe24 and XFe96 microplates were coated with poly lysin-D, $35 \mu\text{l}$ (XFe24) or $15 \mu\text{l}$ (XFe96) one day before seeding. At the day of the experiment, cells were treated with CB839 at 1 or $5 \mu\text{M}$ for 4h, then resuspended in OXPPOS medium containing DMEM (D5030, Sigma-Aldrich), 25 mM glucose, 2 mM L-glutamine, and 1mM sodium pyruvate). Cells were seeded at $250,000/100 \mu\text{l.well}^{-1}$ (XFe24 plate) or $75,000/50 \mu\text{l.well}^{-1}$ (XFe96 plate). Cell plates were centrifuged twice at low speed ($160g$, 1 min) before incubated in a $37^\circ\text{C}/\text{non-CO}_2$ incubator for at least 30 minutes to allow for temperature and pH equilibration prior to the start of an assay. Next, $400 \mu\text{l}$ (XFe24) or $100 \mu\text{l}$ (XFe96) of warm OXPPOS medium was added to each well of the cell plates. Based on the desired redout compounds were prepared at appropriate concentrations. A volume of $75 \mu\text{l}$ (XFe24) or $20 \mu\text{l}$ (XFe96) was added to each injection portals. XFe analyzer settings for OXPPOS measurement: Oligomycin (1 μM), FCCP (0.81-1.72), Antimycin A + Rotenone (1 μM). For the Glutamine oxidation, the assay medium was the base medium without any exogenous fuel substrate. 2mM of Glutamine was injected to initiate glutamine oxidation. CB-839 injection was included in this protocol at 1 or $5 \mu\text{M}$. For ECAR measurement, the assay medium consists of OXPPOS medium-glucose free. 10mM of glucose was injected to initiate glycolysis followed by Oligomycin (2 μM) and then 100mM of 2-DG. OCR and ECAR were reported as absolute rates (pmol/min for OCR and mpH/min for ECAR). In all protocols Hoechst 33342 (Thermo Scientific) Fluorescent Stain was added to portal D at final concentration of 35mM. Metabolic rate was normalized to cell count and data was analyzed with the software Wave (version 2.2.0, Seahorse Bioscience) for further visual presence.

Mitochondrial superoxide membrane potential ($\Delta\Psi$) measurements

Cells were seeded in 6-well plates at a density of 0.9×10^6 cells/well; cells were exposed to single or combination drug treatments as indicated. After the indicated time of incubation, Cells were stained with MitoSOX™ Red Mitochondrial Superoxide Indicator (2.5 μM) (CAT No: M36008, Thermo Fisher) and SYTOX blue (1 μM) (S34857, Thermo Fisher) to measure mitochondrial reactive oxygen species. To measure mitochondrial membrane potential, we used tetramethylrhodamine ethyl ester TMRE (200nM) (ab113852, Abcam). Labeling was done according to the manufacturer's instructions. Fluorescence intensity was measured by flow cytometry. Experiments were performed in triplicate. The results were processed using Kaluza software 2.2 (Beckman Coulter).

CE-MS spectrometry

For the metabolome analysis, U266/Ctrl and U266/MYC cell lines treated with CB-839 1 μM for 48h were prepared in triplicates. The absolute concentration of 116 metabolites was measured using capillary electrophoresis mass spectrometry (CE-TOFMS and CE-QqQMS) in the cation and anion analysis modes for analyzing cationic and anionic metabolites, respectively by the metabolome analysis package Carcinoscope provided by Human Metabolome Technologies (HMT). Samples were prepared following HMT's Sample Preparation Protocol. Briefly, (6×10^6 cells/sample) was used for the extraction of intracellular metabolites. Cells were collected from 100mm plate and washed twice using washing solution (5% mannitol). The cells were then treated with 800 μL of methanol and vortex for 30 s in order to inactivate the enzymes. Next, the cell extract was treated with 550 μL of Milli-Q water containing internal standard (H3304-1002, Human Metabolome Technologies, Inc., Tsuruoka, Japan) and vortex for another 30 s. The extract was obtained and centrifuged at $2300 \times g$ and 4°C for 5 min and then 350 μL of upper aqueous layer was centrifugally filtered through a pre-washed ULTRAFREE MC PLHCC centrifugal filter units (provided by HMT) at $9100 \times g$ and 4°C for 90 min. Samples were evaporated under vacuum conditions at room temperature 1500 rpm, 1000 Pa, 2–3 h (until no liquid remains in the filter cup).

Lentiviral infection and GLS1 knockdown

To generate cells stably overexpress MYC, U266 and Loucy cell lines were transduced with EF1A-C-MYC (PLV-10010-50, Cellomics Technology, LLC) or EF1A-Vector Control lentivirus (PLV-10074-50, Cellomics Technology, LLC). Cells were plated at 50,000 cell per well and transduced over 8 hours at a multiplicity of infection (MOI) 10 in a growth media supplemented with 2 µg/mL Polybrene (Santa Cruz). After 72 hours, cells were selected in medium containing Puromycin (InvivoGen). Inducible lentiviruse short hairpin RNA (shRNA) encoding shRNA targeting GLS1 were purchased from FenicsBIO: shGLS1-1 (tet,Hyg): ATAGGATATTACTTAAAGAAA; shGLS1-2 (tet,Hyg): TGCTAGACAAAGATCTTTTAA; control shRNA (tet,Hyg) (SH-tet-C02). After 72 h, cells were selected in medium containing Hygromycin (InvivoGen). Doxycycline (Med ChemExpress) was used to induce shRNA expression.

In silico

Searching for vulnerabilities associated with MYC overexpression in MM we performed in silico analyses based on a Genome-scale pooled shRNA screens (Achilles) to identify genes essential for the proliferation of 236 cancer cell lines. These screens were performed using a lentivirally delivered pool of 50,529 shRNAs targeting 9273 genes. We correlated the shRNA sensitivity profile with MYC expression values across the 236 cell lines from CCLE database (Affymetrix U133+2 expression array). Each data point represents the abundance of one shRNA construct within one cell line as compared with the initial abundance of that shRNA construct in the initial plasmid DNA pool. To define MYC gene signature we used a subgroup of genes regulated by MYC identified as hallmark_MYC_targets_v2 (https://www.gsea-msigdb.org/gsea/msigdb/cards/HALLMARK_MYC_TARGETS_V2).

RNA-Sequencing

Total RNA was isolated from U266/Control and U266/MYC cells using RNeasy Mini Kit (Qiagen) according to manufacturer's protocol and evaluated for quantity and quality by NanoDrop spectrophotometer. A starting amount of 500 ng of RNA was used to prepare poly-A enriched, single barcoded libraries using the NEBNext® Ultra™ RNA Library Prep Kit (New England Biolabs). Quality control of the libraries was evaluated by Bioanalyzer analysis with High Sensitivity chips (Agilent Technologies). Sequencing was performed on a HiSeq 4000 (Illumina, CA, USA) by 2 X 50 bp paired end reads at the Biopolymers Facility of Harvard Medical School. We used Bcbio_nextgen (<https://github.com/chapmanb/bcbio-nextgen/>) to process the RNA-seq data. Briefly, cutadapt (<https://github.com/marcelm/cutadapt/>) was used to trim adapters; trimmed reads were aligned to Human reference genome (GRCh37) with tophat2; read count for each gene was calculated by HT-seq. Genes with low expression (TPM < 1 across all samples) were filtered out. The RNA-seq data are available in the Gene Expression Omnibus (GEO) under the accession number GSE241948. Gene set enrichment analysis (GSEA) was used to identify significantly enriched pathways, with false discovery rate (FDR) < 0.25 and p value < 0.05. Gene sets were downloaded from the Broad Institute's MSigDB (<http://www.broadinstitute.org/gsea/index.jsp>).

TMT spectrometry

Samples were lysed in a buffer consisting of 50 mM Tris (pH 8.5), 8 M urea, 1% SDS, supplemented with protease and phosphatase inhibitors. Protein quantification was performed using Pierce™ Micro BCA Protein Assay (Thermo Scientific) according to the manufacture protocol. Disulfide bonds of the lysates were then reduced with and dithiothreitol (10mM) and the sulfhydryl groups were alkylated with iodoacetamide (10mM) and methanol/chloroform-precipitated and reconstituted in 100µl HEPES pH 8.5. Afterwards, proteins were digested with LysC (1:50; enzyme:protein) followed by digestion with trypsin (1:50; enzyme:protein) before quantifying, and 100 µg of the peptides of each sample was labeled with TMT reagent. Tandem mass tag reagents (Thermo Fisher Scientific) were dissolved according to manufacturer's instructions. Samples were sent for TMT-based mass spectrometry and further processed at the Thermo Fisher Center for Multiplexed Proteomics (TCMP) facility at Harvard Medical School.

In vivo study

Female SCID/CB.17 mice (n=6 per group) (Charles River Laboratories; 6 weeks-old, 17–20 g) implanted with MM.1S-GFP-Luc⁺ cells (5 x 10⁶ cells injected intravenously). After engraftment, the mice were randomly assigned into four groups based on BLI values and treated with vehicle control, 200 mg/kg CB-839 prepared in [25% (w/v) hydroxypropyl-b-cyclodextrin (HPBCD; MedChemExpress) in 10 mmol/L citrate (Sigma-Aldrich), pH 2 (p.o., b.i.d.)]. 10 mg/kg FK-866 prepared in 20% (w/v) hydroxypropyl-b-cyclodextrin (HPBCD; MedChemExpress) in saline (Aguettant) administrated by intraperitoneal injection twice daily for 4 days, repeated for two weeks followed by single IP injection daily for 4 days weekly repeated over the indicated times or a combination of CB-839 and FK-866 in which each compound was administrated at the same dose and scheduled as single agents. For BLI, mice were injected with 150 mg/kg of D-Luciferin (PerkinElmer), intraperitoneally. After 5 minutes, mice were anesthetized with 2% isoflurane for 5 more minutes; then they were transferred to the chamber of Xenogen IVIS 50 BLI system (Caliper Life Science), placed with their abdomen toward the camera, and imaged on auto exposure. Using Living Image 2.5 software, regions of interest (ROI) were identified around the tumor and relative photon emission (in photons per second per square centimeter per steradian (p/s/cm²/sr)) of the tumor was measured.

QUANTIFICATION AND STATISTICAL ANALYSIS

Data are reported as means ± SEM of at least three independent experiments. Unpaired Student's t test was used to compare two independent groups and multiple-group comparisons were performed using one-way analysis of variance (ANOVA) with Tukey's correction unless

otherwise stated. GraphPad Prism 7 (GraphPad Software Inc.) and Microsoft Excel were used to generate graphs and statistical analysis. ns, not significant; * $P < 0.05$, ** $P < 0.01$, *** $P < 0.001$ and **** $P < 0.0001$. Patients' expression profiles from (MMRF-CoMMpass (<https://portal.gdc.cancer.gov/projects/MMRF-COMMPASS>), (GSE4452)) with the highest and lowest MYC expression were selected. Hem cell lines (n=169) from CCLE were grouped into MYC high and MYC low groups based on the MYC expression above or below the mean value. GSEA was performed using GSEA 4.3.1 (<https://www.gsea-msigdb.org/gsea/doc/GSEAUserGuideFrame.html>). Different gene sets were tested for their enrichment in patient datasets, CCLE as well as U266/Ctrl versus U266/MYC. Gene sets with significant enrichment in MYC OE cells or patients by GSEA were selected on the basis of $P < 0.05$ and q value < 0.25 . For the generation of synergy maps, SynergyFinder (version 3.0) was used, testing was performed using drug-response matrices. Synergy scores were then calculated using Zero Interaction Potency (ZIP) reference model. Based on the algorithm, synergy scores of >10 were considered synergistic, while scores < -10 were considered antagonistic and scores between -10 and 10 were considered additive. For the *in vivo* part, the overall survival was analyzed by Kaplan-Meier curve, and statistical significance was determined by the log-rank test with Bonferroni's correction.